Multiseasonal Predictions with a Coupled Tropical Ocean Global Atmosphere System

Ben P. Kirtman
J. Shukla
Bohua Huang
Zhengxin Zhu
Edwin K. Schneider

Center for Ocean-Land-Atmosphere Studies
Institute of Global Environment and Society, Inc.
4041 Powder Mill Road., Suite 302
Calverton, MD
20705-3106
U.S.A.

June, 1995

Submitted to *Monthly Weather Review*

Abstract

The Center for Ocean-Land-Atmosphere Studies anomaly coupled prediction system, using a sophisticated dynamical model of the tropical Pacific Ocean and the global atmosphere is described. The resolution of the component models is moderate with the atmospheric spectral model truncated at triangular total wavenumber 30 and 18 vertical levels. The ocean model is a Pacific basin model with 0.5° latitude and 1.5 longitude resolution in the wave guide and 20 vertical levels. The performance of the uncoupled component models motivates the anomaly coupling strategy and has lead to the development of a simple empirical technique for converting the 850 mb zonal wind into a zonal surface stress that is used in the prediction experiments described here. In developing ocean initial conditions, an iterative procedure that assimilates the zonal wind stress based on the simulated sea surface temperature anomaly error is applied. Based on a sample of thirty 18 month hindcasts, the predictions have useful skill in the NINO3 region for at least 12 months. The systematic error of the predictions is shown to be relatively small because the ocean initial conditions are in reasonable equilibrium with the ocean model. Finally, composites of the warm and cold El Niño Southern Oscillation (ENSO) events indicate that the model simulates the basic features of ENSO, but there are errors in the horizontal structure of the sea surface temperature anomaly that potentially limit the predictability of the model.

1.0 Introduction

The most well known interaction between the atmosphere and the ocean is the large interannual variation in sea surface temperature, circulation and rainfall in the tropical Pacific. It is now commonly understood that this interannual variation is a manifestation of a coupled ocean-atmosphere instability that is referred to as El Niño and the Southern Oscillation (ENSO; Philander, 1990), and it offers the greatest potential for useful seasonal to interannual climate predictions. In recent years, there have been a number of attempts to capitalize on the predictability of ENSO with different statistical and dynamical models (Cane and Zebiak, 1985; Cane and Zebiak, 1987; Cane et al., 1986; Leetmaa and Ji 1989; Ji et al., 1994a; Balmaseda et al., 1994; Barnston and Ropelewski, 1992; Kleeman 1993; Barnett et al., 1993; Barnett et al., 1994 among others). The various forecasting methods fall into four categories, one of which is purely statistical. The remaining three methods are either purely dynamical or are a combination of dynamical and statistical methods. The intermediate coupled model (ICM) approach is dynamically based and uses simplified models of the ocean and atmosphere (Cane et al., 1986; Zebiak and Cane, 1987; Kleeman, 1993; among others). The hybrid coupled models (HCM) generally use ocean general circulation models (OGCM) and either a simplified dynamical or statistical atmosphere model (Neelin, 1990; Latiff and Villwock, 1990; Jin and Neelin, 1993a and 1993b; Barnett et al., 1993; Graham and Barnett, 1995). The coupled general circulation model approach (CGCM) uses a dynamical OGCM and an atmospheric general circulation model (AGCM). The CGCM method of seasonal to interannual climate predictions is advanced in this paper and a CGCM strategy is also used for operational prediction at the National Meteorological Center (NMC, Ji et al., 1994b). Latif et al. (1994) provide a comprehensive review of ENSO prediction studies.

The ICM approach was pioneered by Cane et al. (1986) and Zebiak and Cane (1987) and is used to produce ENSO forecasts operationally. The forecast system used in Zebiak and Cane (1987), hereafter referred to as ZC, uses a simple Gill (1980) type atmosphere and a one active layer ocean model. Over all initial times, the eastern equatorial Pacific SSTA forecasts were skillful out to a year, but there was also substantial dependence of forecast skill on the initial time of the forecast. Forecasts initialized in January had the shortest predictive lead time while those initialized in April had the longest useful lead. More recently, Chen et al. (1995) have introduced an initialization procedure to the ZC coupled system that dramatically improves the eastern equatorial Pacific SSTA forecasts, particularly for predictions initialized during the 1980's. However, during more recent events, the predictive skill is not much different from the ZC system without the new initialization (Zebiak, personal communication). In the results of Chen et al., (1995) the sensitive dependence of forecast skill on initial time was eliminated. A ZC type model has also been used by Kleeman (1993) and Kleeman et al. (1995) for forecasting and data assimilation experiments. The ICM method has also been employed to study the predictability of the coupled system (Goswami and Shukla, 1991a and 1991b; Blumenthal, 1991; Jin et al., 1994).

The HCM approach has been used in a number of mechanistic studies (Neelin, 1990; Latif and Villwock, 1990; Jin and Neelin, 1993a; Neelin and Jin, 1993; Jin and Neelin, 1993b) and in prediction studies (Barnett et al., 1993; Graham and Barnett, 1995; Barnett et al., 1994). The motivation behind the HCM is that the predictive memory of the coupled system lies in the ocean thermal structure and the atmospheric response is in equilibrium with the ocean. Therefore, the HCM system focuses on the evolution of the ocean and the atmosphere is treated as a rapidly adjusting component of the coupled system.

The CGCM approach has received considerable attention in mechanistic and simulation studies (Philander et al., 1992; Latif et al., 1993a and 1993b; Mechoso et al., 1995; among others). In the prediction mode, there have only been a few attempts (Latif et al., 1993b; Miyakoda personal communication; Leetmaa and Ji, 1989; Ji et al., 1994a and 1994b). The NMC effort (Leetmaa and Ji, 1989; Ji et al., 1994a and 1994b), like the Geophysical Fluid Dynamics Laboratory (GFDL) effort (Miyakoda personal communication), includes a sophisticated ocean data assimilation system to initialize the forecasts (Ji et al., 1995a and 1995b). In a pilot project at the Center for Ocean-Land-Atmosphere Studies (COLA), Zhu and Schneider (1995) considered the anomaly coupled CGCM approach. The prediction model is considered anomaly coupled because the component models predict the total field but the coupling procedure is to exchange only the predicted anomalies plus a prescribed climatology at the interface of the ocean and the atmosphere model. The atmosphere and ocean components of the coupled model presented here are similar to those used at NMC; however, the coupling strategy and the development of ocean initial conditions differ substantially.

The remainder of this paper is as follows. Section 2 describes the component atmosphere and ocean models. Section 3 discusses the coupling strategy and how the empirical 850 mb zonal wind to zonal wind stress correction is applied in the prediction experiments. The development of initial conditions is based on an iterative procedure that is presented in Section 4. The thirty 18 month predictions, their systematic errors and skill are described in Section 5. Section 6 presents warm and cold predicted ENSO composites. Finally, Section 7 contains a summary and some concluding remarks.

2.0 The Component Models

The ocean and atmosphere models used in this study are described below. The atmospheric model has been used in a number of ENSO related predictability studies (Fennessy et al., 1994, Fennessy and Shukla, 1991). The ocean model has also been used for ENSO studies and has been shown to give reasonable interannual variability (Schneider et al., 1995; Huang and Schneider, 1995a; Kirtman et al., 1995).

2.1 The Ocean Model

The ocean model used in this study is a Pacific basin model adapted from the GFDL Modular Ocean Model (Bryan and Lewis, 1979; Rosati and Miyakoda, 1988; Pacanowski et al., 1993) and throughout this paper will be referred to as the GFDL ocean model. This model is a finite difference treatment of the primitive equations of motion using the Boussinesq and hydrostatic approximations in spherical coordinates. The model includes nonlinear vertical mixing of heat, salinity and momentum that is Richardson number dependent (Pacanowski and Philander, 1981), and horizontal mixing of momentum. The domain of the ocean model is restricted to the Pacific basin (30°S-45°N and 130°E-80°W). The zonal resolution is 1.5° and, in the deep tropics (10°S-10°N), the meridional resolution is 0.5° linearly increasing to 1.5° at 20° S and 20° N. There are 20 vertical levels to a maximum depth of 4000 m and the top 16 levels are between 0-400 m. This configuration was used in the study of Huang and Schneider (1995) and Kirtman et al. (1995).

The heat flux calculated by the AGCM has serious systematic errors and is not used in the coupling. Instead, a parameterized heat flux composed of radiative, sensible and evaporative components is used for the coupled predictions and the uncoupled simulations. The radiative fluxes

are divided into solar and terrestrial parts. The monthly mean climatological solar insolation is given by Oberhuber (1988) based on the Comprehensive Ocean Atmosphere Data Set (COADS). The other components are parameterized in terms of the climatological monthly mean air temperature and the model simulated sea surface temperature (SST). The formulation of the long wave radiation is taken from Rosati and Miyakoda (1988), without the effects of cloudiness. The sensible and latent heat fluxes are parameterized by bulk turbulent transfer formulae with parameters given by Philander and Pacanowski (1986). A constant relative humidity of 0.8 is used in the bulk formula to calculate the evaporative heat flux. The surface wind speed for calculating the sensible and latent heat fluxes is determined from the prescribed wind stress forcing using the bulk formula and a drag coefficient of 1.4×10^{-3}. Surface salinity is damped to its climatological monthly mean with a damping time of 50 days. The formulation of the heat and salinity fluxes is the same as that used by Huang and Schneider (1995) and Kirtman et al. (1995). The horizontal diffusion coefficient is taken to be 2×10^7 cm^2 sec^{-1}.

One of the limitations of the forced ocean model experiments and the coupled prediction experiments presented here is in the heat flux formulation. It is fairly well known that this heat flux formulation acts as a damping or relaxation of the simulated SST anomaly (SSTA; Schneider et al., 1995a). Therefore, since both the prediction experiments and the uncoupled ocean experiments use this simple parameterized formulation of the heat flux, the bulk of the SSTA variability is due to the wind stress alone.

The observed wind stress forcing used here was constructed from the Florida State University (FSU) psuedostress. The data come from analyzing tropical Pacific ship and station measurements and are subjectively analyzed to a 2°x 2° grid as described in Goldenberg and O'Brien (1981). The

psuedostress was converted to a wind stress by assuming a constant air density of 1.25×10^{-3} g cm^{-3} and a drag coefficient based on the formulation of Trenberth et al. (1990). The data available are for monthly means from January 1964 to September 1994.

2.2 The Atmospheric Model

The atmospheric model used in the experiments described here is the COLA AGCM. Only a very brief description of the AGCM is provided here. More details can be found in Schneider and Kinter (1994), Xue et al. (1991) and Kinter et al. (1988). The model is a global spectral model with triangular truncation at wavenumber 30. There are 18 unevenly spaced σ coordinate vertical levels. The model includes the simplified biosphere model over land described in Xue et al. (1991); the parameterization of the solar radiation is after Lacis and Hansen (1974); and the terrestrial radiation follows Harshvardhan et al. (1987). The deep convection scheme incorporates a modified version of the Kuo (1965) scheme and the shallow convection follows Tiedtke (1984). There is a second order turbulent closure scheme for subgrid scale exchanges of heat, momentum, and moisture as in Miyakoda and Sirutis (1977) and Mellor and Yamada (1982) at their closure level 2.0. Surface wave drag and the vertical distribution of the wave drag due to vertically propagating gravity waves is parameterized following the procedure by Pierrehumbert (1987), Palmer et al. (1986) and Helfand et al. (1987) (see Kirtman et al., 1993 for details).

The AGCM experiments described here use prescribed SST after either Reynolds (1988) for the period 1982-1994 or SST provided by C. K. Folland of the Hadley Center for the period 1948-1981. The SSTA for the entire record (1948-1994) is computed as the deviation from the mean annual cycle computed separately for both SST data sets. In other words there are different SST

climatologies for the Reynolds (1988) data and the Hadley Center data and the SSTA is computed with respect to the appropriate climatology. The AGCM wind and wind stress data used in the following experiments come from an extended integration of the AGCM using the prescribed SST for 1948-1994.

3.0 The Coupling Strategy

As mentioned earlier, we employ an anomaly coupling strategy. The model ocean and atmosphere exchange predicted anomalies which are computed relative to model climatologies, while the climatology upon which the anomalies are superimposed is specified by observations. The model climatologies are defined by separate uncoupled extended simulations of the ocean and atmosphere models. In the case of the atmosphere, the model climatology is computed from a 45 year (1949-1994) integration with specified observed SST, and, in the case of the ocean we use a 30 year (1964-1994) integration with prescribed FSU wind stress and parameterized heat flux as described in Section 2.

In the prediction mode, the anomaly coupling strategy may be viewed as follows. Given an SST field, the AGCM predicts a wind stress field (τ). The AGCM wind stress climatology (τ_c), computed from the 45 year uncoupled simulation described above, is then subtracted and the anomaly ($\tau_a=\tau-\tau_c$) is added to the observed climatology (τ_o) so that the predicted total wind stress field (τ_p) used to force the ocean model is given by

$$\tau_p = \tau - \tau_c + \tau_o \ .$$

Given τ_p, the ocean model produces an SST field (T). The ocean model SST climatology (T_c), calculated from the 30 year uncoupled simulation described above, is then subtracted and the observed climatology (T_o) is added so that the predicted total SST (T_p) is given by

$$T_p = T - T_c + T_o \ .$$

The observed wind stress climatology (τ_o) is computed from the 30 years of FSU wind stress data and the observed SST climatology (T_o) is calculated from the Reynolds (1988) blended analysis.

The ocean and atmosphere exchange information once per simulated day and a thirty day running mean is applied to both the wind stress anomaly and the SSTA. The formulation of the parameterized heat flux for both the ocean and atmosphere components of the coupled model is the same as in the uncoupled simulations.

The motivation for the anomaly coupling strategy is the errors found in the climatologies of uncoupled simulations of the ocean and atmosphere models. In addition, errors in the annual cycle that would affect ENSO predictions were noted in an extended integration of the directly coupled model (see Mechoso et al., 1995; Schneider et al., 1995b).

Figure 1 shows three repeated annual cycles of zonal wind stress along the equator calculated from the 45 year simulation of the uncoupled AGCM (τ_c). The FSU annual cycle (τ_o) and the error in the simulated annual cycle (τ_c- τ_o) are also shown in Fig. 1. The model captures the broad features of the annual cycle with easterlies throughout most of the equatorial Pacific. The simulated annual cycle of surface stress has an apparent spurious tendency for westward propagation much like the annual cycle in the observed SST (see Fig. 2). The annual cycle of the FSU data shows little propagation suggesting that the AGCM wind stress may be too sensitive to the lower boundary condition of SST. In the error field, the westward propagation of the AGCM annual cycle is seen as westerly errors that have a maximum of 0.3 dynes cm^{-2} in the central Pacific during boreal spring that gradually move to the western Pacific in late summer to early fall. If full coupling were used, these errors would lead to warm ENSO like conditions each boreal spring. In the western Pacific, the errors are largest in the boreal winter when the AGCM fails to capture the intensity of the

westerlies. In the eastern Pacific, the errors tend to be somewhat smaller with the model having too much easterly momentum. By design, the anomaly coupling strategy removes the error in the annual cycle, however, as shown in the next section additional modifications to the wind stress anomaly are required.

Figure 2 shows the mean annual cycle of the SST along the equator as simulated by the OGCM with prescribed FSU wind stress forcing (T_c). The observed SST (T_o, Reynolds, 1988) and the SST error (T_c-T_o) are also shown in Fig. 2. The OGCM captures the phase and, to some degree, the westward propagation of the annual cycle. Throughout most of the basin along the equator the simulated annual cycle is colder than observed. The error is largest in the eastern Pacific where the SST is too cold by 2°K during most of the year. In the western Pacific, the error is relatively small; however, the SST errors are sufficiently large to restrict convection from shifting eastward and thus artificially reduce the potential for interannual variability.

3.1 Surface Wind Stress Anomaly

While the general form of our coupling strategy is similar to that used by NMC, there are some important differences in the details. For example, noting serious problems with the surface wind stress anomalies simulated by the AGCM, Ji et al. (1994a) tuned the convective parameterization and the vertical diffusion. Similar problems with the COLA AGCM wind stress anomalies were noted by Huang and Schneider (1995), Huang and Shukla (1995) and Kirtman et al. (1995). Here, we have taken a different, and primarily empirical, approach to improving the momentum flux which was first discussed by Huang and Shukla (1995) and modified to include the annual cycle by Kirtman et al. (1995).

The problem with the simulated wind stress seems to be caused by errors in the boundary layer parameterization. This conjecture is based on the fact that relatively large temporal correlations are observed between the ECMWF zonal wind anomalies and the COLA AGCM zonal wind anomalies at 850 mb. On the other hand, the same correlation at the surface is quite low. Motivated by the high correlation at the top of the boundary layer, Huang and Shukla (1995) derived an empirical relation between the AGCM 850 mb zonal wind and the zonal surface stress. Kirtman et al. (1995) modified the Huang and Shukla (1995) formulation to include a longer record of observed data and the annual cycle. This empirical zonal wind stress formulation may be interpreted as an intermediate statistical model that includes dynamical constraints from the AGCM. The difference between this wind stress and those derived from statistical models, such as the one used in Barnett et al. (1993), is that it is explicitly constrained by the AGCM dynamics and physics. This approach also differs from that of Ji et al. (1994a) in that they try to improve the simulation of surface stress by tuning the physical parameterizations, whereas we bypass the errors in the boundary layer by

using the 850 mb zonal winds. Ultimately, the formulation of both the boundary layer and the convection in the model must be improved to make further progress in predicting the coupled ocean-atmosphere system.

The procedure for calculating the surface stress from the 850 mb zonal winds uses a linear least squares fit between the AGCM 850 mb zonal wind and the FSU observed surface stress. The least squares fit defines the coefficients α and β such that

$$\tau_x = \alpha + \beta U_{850}$$

where τ_x is the zonal wind stress calculated from the 850 mb zonal wind. The coefficients α and β are functions of latitude, longitude and month of the year so that the annual cycle is included in the formulation for zonal wind stress. Thirty years (1964-1993) of FSU data are used in calculating the least squares fit that gives 12 values of α and β for each AGCM grid point.

Figures 3a and 3b show time longitude cross sections of the zonal wind stress anomaly (mean annual cycle removed) along the equator in the Pacific calculated from the AGCM forced with prescribed SST and the FSU analysis. In comparing the two wind stress fields, some problems with the AGCM wind stress anomalies are apparent. The AGCM anomaly is about a factor of two smaller than the FSU anomaly. The AGCM anomaly is too narrowly confined to the western extreme of the Pacific basin. Moreover, the weakening of the westerly anomaly during the Northern Hemisphere spring season leads to cold SSTA that serves to interrupt the warm ENSO events along the equator (Huang and Schneider, 1995; Kirtman et al., 1995).

Figure 3c shows the zonal wind stress calculated from the 850 mb zonal wind, hereinafter referred to as the statistically corrected zonal wind stress. In general the wind stress calculated from the AGCM 850 mb zonal wind is smoother than both the AGCM surface stress and the FSU data. There is a tendency for the statistically corrected zonal wind stress anomaly, to be shifted to the east of both the FSU data and the surface wind stress anomaly. There are also some important differences in the details of the individual easterly and westerly anomaly events. For example, in the statistically corrected zonal wind stress anomaly, there is a second westerly maximum in late 1987 which is nearly absent in the FSU data. In the FSU data, there is a strong easterly anomaly in early 1984 and a somewhat weaker anomaly in early 1985. The relative strength of the easterly anomalies in 1984 and 1985 is reversed in the statistically corrected zonal wind stress.

The horizontal structure of a composite wind stress anomaly for the three wind stress fields is presented in Figs. 4a-4c. The composite is calculated by taking the averaged anomaly for December-February 1982-83, 1986-87 and 1991-92. The most outstanding difference among the three composites is the degree of organization of the westerly anomalies. The AGCM surface wind stress is dominated by northerly flow along the equator turning to the west in the southern Hemisphere with the maximum westerly anomaly at 5°S. The FSU data also has a strong northerly component along the equator but a westerly anomaly is still apparent. In the statistically corrected wind stress data, the northerly component is weaker as the anomaly is dominated by westerly flow on both sides of the equator.

There are features in the FSU and AGCM surface wind stress composite anomaly that are absent from the statistically corrected wind stress composite anomaly. For example, the northeasterly anomaly in the eastern Pacific and the equatorward flow in the south central Pacific are missing. The

anomaly in the statistically corrected wind stress is smoother and more zonally oriented than either the FSU or the AGCM surface wind stress anomaly. In terms of simulating ENSO with this ocean model, the statistically corrected zonal wind stress does better because it isolates the slow ENSO mode in the 850 mb zonal wind; however, it does not capture many of the observed features in the FSU data that are simulated by the AGCM surface stress.

A straightforward way to objectively determine which of these three wind stress anomaly products is best for coupling with our ocean model is to force the ocean model with these wind stress fields. In three parallel experiments we used the anomaly fields in Figs. 3a-3c superimposed on the same wind stress climatology to force the ocean model. The monthly mean climatological wind stress was calculated from the FSU data in all three experiments.

Figures 5a-5d show the simulated SSTA along the equator for the three experiments along with the Reynolds (1988) observed anomaly. All three simulation capture the observed interannual variability with varying degrees of fidelity. Temporal correlations and root mean square errors (see Kirtman et al., 1995) calculated over the complete record 1964-1994 indicate that the AGCM surface wind stress gives the poorest simulation and that the AGCM statistically corrected wind stress gives a better simulation of the interannual variability than the FSU data. All three simulations fail to capture the strength of the oscillations specifically in the eastern Pacific, although the simulation in the east becomes progressively better in going from Fig. 5a to Fig. 5c. In the AGCM surface wind stress simulation, there are cold interruptions during both the 1983 and 1987 warm event. These interruptions are linked to a southward shift of the wind stress anomaly which is similar to the composite shown in Fig. 4a. Huang and Schneider (1995) have shown that this southward shift of

the wind stress anomaly is connected to an erroneous southward shift of the AGCM climatological intertropical convergence zone (ITCZ).

The differences in the individual ENSO events are important particularly if the simulations are used as initial conditions for coupled forecasts. For example, during the second half of 1987, the FSU simulation gives near normal SST, whereas both Fig. 5a and Fig. 5b indicate a secondary warming as in the observations although weaker. Coupled forecasts initialized with the FSU simulation in middle to late 1987 fail to capture warm SSTA that persists through January 1988 in the observations. The FSU simulation also has a tendency to produce a cooling trend about 3 months too early in the eastern Pacific for the 1988 cold event. Both the FSU and the statistically corrected wind stress simulation have relatively cold temperatures in the latter half of 1983 that are too strong compared to the observations and too weak in 1984-85.

A composite SSTA calculated in the same way as in Fig. 4a-4c is shown in Fig. 6a-6d. All three simulation composites are weak in the eastern Pacific, and the AGCM surface stress yields the weakest response. There is a local maximum in the central Pacific centered around 165°W in the simulations that is absent from the observations. The meridional scale of the simulated anomaly is also severely truncated in comparison with the observations. While it is clear that the AGCM statistically corrected wind stress gives a better simulation of the SSTA than the AGCM surface stress, neither the FSU nor the statistically corrected wind stress simulation gives sufficiently accurate initial conditions for coupled prediction.

4.0 Initial Conditions

In the previous section we showed that, in many ways, the zonal wind stress calculated from the AGCM 850 mb wind produces an SSTA simulation superior to both the AGCM surface wind stress and the FSU wind stress. However, in terms of coupled prediction, none of the three simulations produces ocean initial states that are sufficiently accurate for coupled forecasts. For example, in January 1988, the Reynolds data indicate that the SST are nearly a degree warmer than normal (see Fig. 5d), whereas, the statistically corrected wind stress simulation gives only a very small region near the date line where SST are above normal (see Fig. 5c). The response to FSU forcing in January 1988 is even worse (see Fig 5b). When using either the statistically corrected wind stress or the FSU wind stress simulation as an initial condition for a coupled forecast, the prediction skill starts off low and then deteriorates.

Motivated by the need to generate better ocean initial conditions without necessarily assimilating sub-surface ocean data, Kirtman et al., (1995) developed an iterative wind stress assimilation procedure. The wind stress is modified to correct the simulated SSTA error. A linear adjustment was applied which was local in both space and time where for each 1°K of SSTA simulation error, the zonal wind stress anomaly was adjusted by 0.1 dynes cm^{-2}. The iteration procedure is to run the OGCM, adjust the zonal wind stress based on the SSTA error and then repeat the process. The final product is a better ocean simulation as measured by the SSTA correlation and the RMSE and possibly a better zonal wind stress anomaly.

There are large spatial and temporal scales associated with the simulated SSTA errors which, by definition of the iteration procedure, translate into wind stress differences among the iterates that are of the same spatial and temporal scales. Figure 7 shows a time longitude cross section of the

zonal wind stress anomaly before and after the iteration is applied. The zeroth iterate or the first guess in the iteration procedure is taken from the statistically corrected zonal wind stress. The dominant difference between the iteration wind stress and the statistically corrected wind stress is a large scale eastward shift of the anomaly. There are several features in the observed SSTA that the statistically corrected wind stress simulation fails to capture and that can be readily identified in the iteration wind stress. For instance, warming in the far eastern Pacific during May 1983 appears as a 0.2 dynes cm^{-2} westerly anomaly. The colder than normal temperatures throughout 1984 and 1985 are associated with a marked eastward broadening of the anomaly in the interation wind stress. Similar changes are noted in the 1987-88 ENSO event.

Figure 8 shows the time longitude cross section of the simulated SSTA associated with the statistically corrected wind stress before and after the iteration is applied. The observed SSTA is also shown in Fig. 8 for comparison. The most pronounced difference between the two simulations is the eastward shift and intensification of the SSTA which brings the simulated SSTA into better agreement with the observed SSTA. The 1982/83 warm event after the first iteration shows a suggestion of a secondary maximum in the far eastern Pacific much like the analysis. Relatively cold SSTA of approximately -1°K persists from mid 1983 through early 1986 in the SST analysis and some improvement can be detected after the adjustment to the wind stress. Perhaps the most impressive improvements occur during the 1987-88 ENSO event when the iteration and the observations indicate positive SSTA in the eastern and east central Pacific for all of 1987, but in the first guess simulation the SST returns to near normal conditions by the middle of 1987. The sharp transition to the 1988 La Niña is also better simulated after the wind stress has been adjusted.

Figure 9 shows the SSTA correlation (with the observed SSTA) before and after the zonal wind stress iteration has been applied. There is an increase in the correlation with a larger region where the observed SSTA and the simulated SSTA have a correlation coefficient greater than 0.6. There are also notable increases in the correlation in the eastern Pacific and portions of the sub-tropical Pacific. Since the iterative wind stress is used as initial conditions, Fig. 9 can also be interpreted as the zero lead time correlation.

5.0 Coupled Forecast Results

We have completed a set of hindcast predictions for the period 1964-1991 using the dynamical ocean-land-atmosphere general circulation model described in the above sections. A hindcast was initialized for each January and July of 1965, 1966, 1970, 1972, 1973, 1974, 1975, 1982, 1983, 1984, 1986, 1987, 1988, 1989 and 1991. These years where chosen to sample warm, cold and normal years. Each hindcast was run for 18 months. The ocean initial conditions for all of these predictions were taken from an uncoupled simulation in which the 850 mb zonal wind was converted into a surface stress and then the iterative wind stress procedure was applied so that both the ocean and atmosphere models are close to equilibrium with the wind stress anomaly and the SSTA, respectively.

To verify the hindcasts of SSTA initialized prior to 1982, we used SST provided by C. K. Folland of the United Kingdom Meteorological Office. After 1982 we used the blended analysis of Reynolds (1988) for verification.

5.1 Systematic Error

One of the main differences between the prediction system presented here and that used by NMC is in the procedure for developing initial conditions. The experience at NMC is that the ocean data assimilation system yields better forecasts, but the forecasts also have larger systematic errors. The experience at NMC identifies both the importance of ocean data assimilation in seasonal to interannual forecasting and the need for ocean model development designed to reduce the systematic errors; in fact, the two problems are coupled and need to be addressed as such. In some sense, the iterative wind stress procedure presented here is a compromise between using ocean data

assimilation and reducing the systematic errors of the forecasts. Typically, when the forecast skill is evaluated in the NINO3 region, the systematic error is removed a posteriori. However, given the highly nonlinear nature of the remote response to tropical forcing, the systematic error will impact the remote forecast in such a way that it cannot be removed in this linear fashion. One of the advantages of the prediction system presented here is that the systematic error is relatively small compared to other similar coupled prediction systems.

The systematic error for the January predictions, for example, is defined as the mean of all 15 anomaly predictions initialized in January. Since each prediction is 18 months in duration, there are 18 months of systematic error. The systematic error is defined as

$$T_{sys} = \frac{1}{N} \sum_{j=1}^{N} (T_p - T_c)$$

where, in this example, the summation is over all forecasts initialized in January and N is the number of forecasts initialized in January. The systematic error is defined in the same way for the forecasts initialized in July.

Figure 10 shows the evolution of the NINO3 (150°W-90°W, 5°S-5°N) systematic error of SST for both the January and July forecasts. These curves can be compared to those in Ji et al. (1994a, see their Fig. 5). Overall the systematic error is smaller in the COLA predictions, but the initial bias is about the same, suggesting that there is little initial shock in the forecasts due to an imbalance of the initial conditions and the ocean model. The systematic error in the COLA prediction system is bounded between ±0.4°C, whereas the absolute value of the NMC error exceeds 0.4°C for most lead times. The extreme systematic error of the NMC model exceeds 1.0°C. Similar

to the behavior of the NMC model, the forecasts initialized in the winter season tend to have the smallest initial systematic errors. The COLA January forecasts have systematic errors that are less than 0.1°C in absolute value for the first 9 months. The evolution of the July forecasts are very similar in structure to the NMC summer forecasts, the warm bias peaks in late fall or early summer and then decreases in both models.

Considering the equatorial Pacific region as a whole, the largest systematic errors occur during the 10th month (October) of the January forecasts and the 8^{h} month (February) of the July forecasts. Figure 11 shows the horizontal structure of these errors. For both sets of initial conditions and all lead times, there are fairly large errors along the eastern boundary which are also apparent in Fig. 11. The January forecasts have their largest cold errors in the eastern Pacific with a sizable region where the absolute error is greater than 0.6°C. In contrast, the July forecasts have their largest errors in the west central Pacific. This error in the July forecasts is most likely an associated with the fact that the wind stress is systematically shifted too far to the west with too strong an SST response in this region. Unfortunately, this SST error also has an associated precipitation (convective heating) error producing an extratropical circulation error that potentially limits the predictability in the extratropics.

5.2 Forecast Skill

The 18 month evolution of the SSTA in the NINO3 region for all the hindcasts is shown in Fig. 12. The systematic error in the predicted SSTA has been removed and the observed NINO3 SSTA is indicated by the bold solid line. It should be noted that the statistical wind stress correction procedure was derived with FSU data for the period 1964-1994 and the prediction experiments

presented here are dependent on the FSU observations. However, the uncoupled performance of the 850 mb wind stress correction was tested on an independent period (1948-1963) and found to give similar improvements over the AGCM surface stress (see Kirtman et al., 1995). Two real predictions, one initialized in July 1994 and the other in January 1995, are also shown. For the most part, the predictions track the observed anomalies for the first 12 months although there are some notable exceptions. The forecasts initialized in January 1974, January 1989 and July 1988 have relatively cold initial states and 6-12 months later produce erroneous warm anomalies when the observed SSTA was returning to near normal conditions. There are similar problems, but with warm initial states, for the forecasts initialized in January 1966 and January 1970.

The NINO3 SSTA correlation and root mean square error (RMSE) is shown in Fig. 13. In addition to the skill of the COLA model, the skill of two other prediction systems (NMC and ZC) is also shown. The skill scores for the other prediction systems were provide by Ji (personal communication) and Zebiak (personal communication), respectively. It should be noted that the verification of the other prediction systems includes different initial times and different sample sizes. The NMC forecasts were initialized each month from October 1983 to February 1993. The ZC predictions are also monthly and are verified for January 1972 through December 1992. Because the verification period and the sample sizes of the three prediction systems differ, the skill scores cannot be quantitatively compared here. Only a qualitative comparison is possible. The intention here is not to identify the best prediction system with this metric, but to demonstrate the rapid progress and the state-of-the-art in forecasting NINO3 temperatures.

With these simple metrics, all the various prediction systems are doing a fairly reasonable job of forecasting NINO3 SSTA. The character of the skill scores associated with the various forecasting approaches, however, varies. The CGCM methods (COLA and NMC) are comparable, with the highest correlations during the earliest part of the forecast period. The skill of CGCM methods also improves significantly with the inclusion of statistical corrections to the surface wind stress forcing. The ICM approach, such as the ZC model, loses skill much less rapidly than the CGCM approach but has initial skill scores that are somewhat lower than the CGCM systems. The most recent results with the ZC model incorporate an initialization scheme that yields remarkably good skill scores out to 20 months (Chen et al., 1995).

The three curves for the COLA anomaly coupled prediction system show improvements over the course of approximately one calendar year. The earliest version of the model (COLA1) did not apply a 30-day running mean to the anomalies (SST and wind stress), did not use the statistically corrected wind stress correction and did not use the iterative wind stress assimilation. In these early prediction experiments the ocean initial conditions were taken from an uncoupled ocean model simulation with prescribed ECMWF wind stress forcing. The second generation of the prediction system (COLA2) incorporated a statistically corrected wind stress that omitted the annual cycle (see Huang and Shukla, 1995, Kirtman et al., 1994) and the 30-day running mean was applied. The third pair of curves (COLA3) gives the correlation and RMSE for the version of the COLA model described here. The correlations (RMSE) have steadily increased (decreased) with changing versions of the model, where, with the most recent version of the model, the correlation remains above 0.6 for lead times up to 12 months.

In controlled experiments, we have examined the sensitivity of a subset of the prediction experiments to the statistically corrected wind stress and the initial conditions that arise for the wind stress iteration. The bulk of the reduction in the error and the increased correlation seen in Fig. 13 is due to the statistically corrected wind stress in improving both ocean initial conditions and the wind stress forcing that is felt by the ocean component of the coupled model. The iteration wind stress initial conditions also improve the correlation and reduce the error particularly in the early part of the forecast period.

6.0 Composite Warm and Cold Events

Similar to the NMC forecasts, the COLA predictions verify somewhat better in the central Pacific than in the eastern Pacific. This is primarily due to the fact that the AGCM wind stress response to the observed SSTA is strongest in the western and west-central Pacific, and the response further to the east is quite weak and often of the wrong sign. The strong response in the central Pacific can be seen in Figs. 14 and 15 where the hindcast and observed SSTA for composite warm (DJF 1965-66, DJF 1972-73, DJF 1982-83 and DJF 1987-88) and for composite cold (DJF 1970-71, DJF 1973-74, DJF 1984-85, and DJF 1988-89) events is plotted. For all the composites we show the forecasts initialized in July so the figures plotted are for lead times of 6-8 months.

The SSTA, zonal wind stress, sea level pressure and precipitation composites show that the predictions contain many of the basic features of ENSO: SSTA in the eastern and central tropical Pacific with accompanying wind stress anomaly, nearly global scale oscillations in the sea level pressure and large-scale shifts in the ITCZ complexes. The composite predictions of the SSTA are slightly too weak in the warm case and too weak by nearly a factor of two in the cold case. In general, the predictions do a better job of capturing the amplitude and meridional extent in the central part of the basin. On the other hand, in the warm and cold events, the predictions capture a suggestion of the anomaly extending along the South American coast in the NINO1 and NINO2 regions. In the observed composites, there are subtropical anomalies of the opposite sign in the western Pacific. The predictions also give anomalies of the opposite sign in the western Pacific but they are confined too close to the equator.

A clear deficiency in the predictions is in the meridional extent of the SSTA. The observed anomaly extends into the subtropics for both the warm and cold events, whereas the predicted SSTA is confined to the region between 5°S and 5°N. Simulating the correct meridional extent may be particularly important in terms of capturing the extratropical atmospheric response, as has been pointed out by Held and Kang (1987) and Held et al. (1989) who find that the extratropical response depends on the extension of the SSTA into the subtropics.

The lack of an extension into the subtropics is due to problems in both the AGCM wind stress and errors in the ocean model. In uncoupled simulations with this ocean model, the meridional extent of the SSTA is also too narrow, and, even the statistically corrected wind stress does not extend far enough off the equator (see Figs. 4 and 6). In the coupled prediction model, these two problems can reinforce each other which leads to further confinement of the predicted anomaly. In other words, a narrow band of SSTA leads to a narrowing of the zonal wind stress anomaly which then leads to even further narrowing of the SSTA. The equatorial confinement of the wind stress anomaly can be seen in Figs. 16 and 17 which show the warm and cold event zonal wind stress anomaly composites. The iteration zonal wind stress composite is also shown for comparison. The anomaly is meridionally truncated in comparison with the assimilated zonal wind stress. There is also the appearance of a weak anomaly of the opposite sign in the eastern Pacific which inhibits the growth of the SSTA in the east. In the warm composite case, the westerly anomaly extends further to the west than the assimilated wind stress in a narrow region along the equator. This is consistent with the erroneous warm tongue in the predicted SSTA and the July systematic error. In multi-decade integrations of this anomaly coupled model, the equatorial confinement and westward expansion of the warm and cold events becomes even more enhanced.

The weak wind stress anomaly is consistent with the sea level pressure anomaly shown in Figs. 18 and 19. For comparison, we show the sea level pressure composite anomaly calculated from a long integration (1948-1995) of the AGCM with observed SST. The simulation of the uncoupled Southern Oscillation Index (SOI) is realistic and the predictions capture the major oscillations of the simulated SOI (not shown). The predictions also capture the broad horizontal structure of the east-west contrast in the Southern Oscillation for both the warm and cold events. However, the zonal gradient of the predicted sea level pressure anomaly is weak in comparison with the uncoupled simulation of the sea level pressure anomaly. Again, the node of the sea level pressure anomaly is shifted westward in the case of the warm events similar to the wind stress anomaly and the SSTA.

The composite precipitation anomaly is shown in Figs. 20 and 21. The uncoupled simulation with observed SST provides a homogeneous precipitation record for comparison. The uncoupled AGCM has a reasonable simulation of tropical and subtropical precipitation anomalies, and it provides a useful measure of what could be simulated from the anomaly coupled model if the predicted SSTA were perfect. In the tropical Pacific, the anomaly coupled model has predicted the basic features of the simulation with reduced rainfall throughout most of the Pacific in the cold composite and enhanced rainfall in the warm composite. There are anomalies in the subtropical Pacific and the remote parts of the tropics for which the simulation and the predictions are consistent. For example, in the warm composite, the uncoupled simulation and the prediction give reduced subtropical rainfall straddling the enhanced rainfall. Rainfall anomalies over Australia, tropical Africa and Brazil also appear to be potentially predictable.

As expected, the uncoupled simulated rainfall anomalies are somewhat stronger than the predicted anomalies. The predicted composite rainfall anomaly is also shifted too far to the west much like the other composites. The extratropical response is sensitive to these structural and amplitude differences. We have formed composites of the 200 mb height anomalies and compared them with the uncoupled simulations (not shown). In the tropics, the agreement is reasonable: the uncoupled simulation and the predictions produce either a warming or a cooling of the tropical troposphere. However, there is little agreement between the simulation and the predictions in the extratropics. Part of the problem is that the AGCM response to tropical heating anomalies is weak and larger ensembles are required to obtain robust extratropical signals.

7.0 Summary and Concluding Remarks

The prediction experiments presented here show that ENSO and ENSO related climate anomalies in the tropics are potentially predictable with complex ocean-land-atmosphere general circulation models. However, the fact that the anomaly coupling strategy was employed and statistical corrections to the wind stress were required indicates that there is ample opportunity to improve the coupling strategy, the component models and, ultimately, the predictions.

Long uncoupled simulations of the ocean and atmosphere component models showed errors in the simulated annual cycles of SST and wind stress, that, in the directly coupled model, lead to large climate drift and weak interannual variability. Based on the performance of the uncoupled component atmosphere and ocean models, we have taken the anomaly CGCM approach for seasonal to interannual climate predictions. Following Huang and Shukla (1995) and Kirtman et al. (1995) we have empirically converted the 850 mb zonal winds into a zonal surface stress for prediction experiments presented here. We have also used the iterative wind stress procedure described in Kirtman et al. (1995) to generate ocean initial conditions. This simple iterative procedure has the advantage that the systematic error of the predictions is relatively small in comparison to sophisticated ocean data assimilation systems; however, we do not see the dramatic increase in predictive skill that is typically obtained with the assimilation of observed sub-surface thermal data.

Based on thirty 18 month hindcast experiments including warm, cold and normal years, the predictions are found to have useful skill up to at least 12 months lead time as measured by the NINO3 SSTA correlation and RMSE. The skills of the two CGCM (COLA and NMC) forecasts are comparable, and, for the early part of the forecast period, the CGCM predictions have larger correlations than the ICM approach, but the ICM approach gives better results for lead times greater

than 12 months. Some of the predictions that started from cold initial states produced erroneous warm anomalies 6-12 months later when the observed SSTA was returning to near normal conditions. In extended integrations of the prediction model, fairly strong biennial oscillations are observed, suggesting that the model has a tendency to oscillate between the extreme ENSO states, consistent with the problems in some of the prediction experiments.

Composites of the warm and cold predicted SSTA show that the meridional structure of the anomaly is too narrow, and there is a tendency to overpredict the anomaly in the central and western Pacific. Composites of the atmospheric response are encouraging, particularly for the rainfall anomalies in the tropical Pacific. The 200 mb extratropical height anomalies are not realistic, indicating that larger ensembles are required and improvements to the atmospheric model must also be made.

The skill of earlier versions of the model without the statistically corrected wind stress or the iterative wind stress assimilation was also briefly discussed. Some sensitivity experiments were also performed that were intended to isolate the relative effects of the statistically corrected wind stress and the iterative wind stress assimilation. In general, the statistically corrected wind stress was shown to give the greatest improvement in the forecasts and the iterative wind stress assimilation improved the forecasts particularly for short lead times.

While the results presented here are encouraging, there are a number of things that need to be improved with the model. The most serious problem is with the horizontal structure of the uncoupled and coupled SSTA. The parameterized heat flux, which acts to damp the SSTA, is a particularly bad formulation off the equator and possibly contributes to this problem. The heat flux into the ocean model needs to be changed to include anomalies from the atmospheric model.

Refinements to the vertical mixing parameterization in the ocean model will also lead to improvements in the meridional structure of the SSTA. There are active research efforts at COLA designed to improve the AGCM tropical boundary layer and the extratropical response to observed SSTA. We need to consider ensemble prediction in order to capture the extratropical response, and we need to sample a larger set of initial conditions in our skill assessment. We are actively pursuing a number of different approaches to ocean data assimilation that are designed to improve the ocean model, the ocean model simulation and the coupled forecasts, without introducing additional systematic error.

Acknowledgments

This research is part of a larger effort at COLA to study the predictability of the coupled system. Members (J. Kinter, L. Marx, D. DeWitt and M. Fennessy) of this group have provided invaluable advise. The extended integrations of the uncoupled AGCM were performed by L. Marx. M. Ji and S. Zebiak provided the skill scores for the NMC and ZC models and we are grateful for there support and comments. We are also thankful to R. Reynolds and C. K. Folland for providing the SST data. L. Kikas assisted in archiving and managing the data. A large amount of computer time for this project was provided though NOAA's Office of Global Programs and we are very grateful to K. Mooney for providing this computer time. This work was supported under NOAA grant NA26-GPO149 and NA46-GPO217 and NSF grant ATM-93021354.

References

Balmaseda, M. A., Anderson, D. L. T. and M. K. Davey, 1994: ENSO prediction using a dynamical ocean coupled to a statistical atmosphere. *Tellus*, **46A**, 497-511.

Barnett, T. P., L. Bengtsson, K. Arpe, M. Flugel, N. Graham, M. Latif, J. Ritchie, E. Roeckner, U. Schulzweida and M. Tyree, 1994: Forecasting global ENSO-related climate anomalies. *Tellus*, **46A**, 381-397.

Barnett, T. P., M. Latif, N. Graham, M. Flugel, S. Pazan, and W. White, 1993: ENSO and ENSO-related predictability. Part I: prediction of equatorial Pacific sea surface temperature with a hybrid coupled ocean-atmosphere model. *J. Climate*, **6**, 1545-1566.

Barnston, A. G. and C. F. Ropelewski, 1992: Prediction of ENSO episodes using canonical correlation analysis. *J. Climate*, **5**, 1316-1345.

Blumenthal, M. B., 1991: Predictability of a coupled ocean atmosphere model. *J. Climate*, **4**, 766-784.

Bryan, K. and L. Lewis, 1979: A water mass model of the world ocean. *J. Geophys. Res.*, **84**, 2503-2517.

Cane, M. A. and S. E. Zebiak, 1987: Predictions of El Niño events using a physical model. In *Atmospheric and Oceanic Variability*, H. Cattle, ed., Royal Meteorological Society Press, 153-182.

Cane, M. A., S. E. Zebiak and S. C. Dolan 1986: Experimental forecasts of El Niño. *Nature*, **321**, 827-832.

Cane, M. A. and S. E. Zebiak, 1985: A theory for El Niño and the southern oscillation. *Science*, **228**, 1085-1087.

Chen, D., S. E. Zebiak, A. J. Busalacchi and M. A. Cane, 1995: An Improved Procedure for El Niño Forecasting. *Science* (submitted).

Fennessy, M. J., J. L. Kinter III, B. P. Kirtman, L. Marx, S. Nigam, E. K. Schneider, J. Shukla, D. Straus, A. Vernekar, Y. Xue and J. Zhou, 1994: The simulated Indian monsoon: A GCM sensitivity study. *J. Climate*, **7**, 33-43.

Fennessy, M. J. and J. Shukla, 1991: A comparison of the impact of the 1982-83 and 1986-87 Pacific SST anomalies on time mean prediction of atmospheric circulation and rainfall. *J. Climate, 4,* 407-423.

Gill, A.E., 1980: Some simple solution for heat induced tropical circulations. *Quart. J. Roy. Meteor. Soc.,* **106**, 447-462.

Goldenberg, S. B., and J.J. O'Brien, 1981: Time and space variability of the tropical Pacific wind stress. *Mon. Wea. Rev.*, **109**, 1190-1207.

Goswami, B. N. and J. Shukla, 1991a: Predictability of a coupled ocean atmosphere model *J. Climate*, **4**, 1-22.

Goswami, B. N. and J. Shukla, 1991b: Predictability and variability of a coupled ocean atmosphere model, *J. Mar. Sys.*, **1,** 271-225.

Graham, N. E. and T. P. Barnett, 1995: ENSO and ENSO related predictability. Part II: Northern Hemisphere 700 mb height predictions based on a hybrid coupled ENSO model. *J. Climate,* **8,** 544-549.

Harshvardhan, R. Davis, D. A. Randall, and T. G. Corsetti, 1987: A fast radiation parameterization for general circulation models. *J. Geophys. Res.*, **92**, 1009-1016.

Held, I. M., and I.-S. Kang, 1987: Barotropic models of the extra-tropical response to El Niño. *J. Atmos. Sci.*, **42,** 3576-3586.

Held, I. M., S. W. Lyons, S. Nigam, 1989: Transients and the extra-tropical response to El Niño. *J. Atmos. Sci.,* **46**, 163-174.

Helfand, H. M., J. C. Jusem, J. Pfaendtner, J. Tenenbaum, and E. Kalney, 1987: The effect of a gravity wave drag parameterization on GLA fourth order GCM forecasts. *NWP Symp. on Short and Medium Range Weather Prediction.* Tokyo, Japan, WMO/IUGG.

Huang, B., and J. Shukla, 1995: Surface wind stress based on AGCM simulated low level winds over the tropical Pacific ocean. *Mon. Wea. Rev.* (submitted).

Huang, B. and E. K. Schneider, 1995: The response of an ocean general circulation model to surface wind stress produced by an atmospheric general circulation model. *Mon. Wea. Rev.* (in press).

Ji. M., A. Leetmaa and J. Derber, 1995a: An ocean analysis system for seasonal to interannual climate studies. *Mon. Wea. Rev.*, **123**, 460-481.

Ji, M., A. Leetmaa, and V. E. Kousky, 1995b: Coupled model forecasts of ENSO during the 1980s and early 1990s at the National Meteorological Center. *Mon. Wea. Rev.* (Submitted).

Ji, M., A. Kumar and A. Leetmaa, 1994a: An experimental coupled forecast system at the National Meteorological Center: Some early results. *Tellus*, **46A**, 398-418.

Ji, M., A. Kumar and A. Leetmaa, 1994b: A multi-season climate forecast system at the National Meteorological Center. *Bull. Amer. Meteor. Soc.*, **75**, 569-577.

Jin, F.-F., J. D. Neelin and M. Ghil, 1994: El Niño on the "Devil's Staircase": Annual subharmonic steps to chaos. *Science*, **264**, 70-72.

Jin, F.-F. and J. D. Neelin, 1993a: Modes of interannual tropical ocean-atmosphere interaction-a unified view. Part I: Numerical results. *J. Atmos. Sci.*, **50**, 3477-3503.

Jin, F.-F. and J. D. Neelin, 1993b: Modes of interannual tropical ocean-atmosphere interaction-a unified view. Part III: Analytical results in fully coupled cases. *J. Atmos. Sci.*, **50**, 3523-3540.

Kinter, J. L. III, J. Shukla, L. Marx and E. K. Schneider, 1988: A simulation of winter and summer circulations with the NMC global spectral model. *J. Atmos. Sci.*, **45**, 2486-2522.

Kirtman, B. P., E. K. Schneider, B. Kirtman, 1995: Model based estimates of equatorial Pacific wind stress. *J. Climate* (submitted).

Kirtman, B. P., B. Huang, Z. Zhu, J. Shukla, E. K. Schneider, L. Marx, D. DeWitt, M. J. Fennessy and J. L. Kinter III, 1994: Coupled Predictions at COLA, *19th Annual Climate Diagnostics Workshop* (College Park, MD).

Kirtman, B. P., A. Vernekar, D. DeWitt and J. Zhou, 1993: Impact of orographic gravity wave drag on extended range forecasts with the COLA-GCM. *Atmosfera*, **6**, 3-24.

Kleeman, R., A. M. Moore and N. R. Smith, 1995: Assimilation of sub-surface thermal data into an intermediate tropical coupled ocean-atmosphere model. *Mon. Wea. Rev.* (in press).

Kleeman, R., 1993: On the dependence of hindcast skill on ocean thermodynamics in a coupled ocean-atmosphere model. *J. Climate*, **6**, 2012-2033.

Kuo, H. L., 1965: On the formation and intensification of tropical cyclones through latent heat release by cumulus convection. *J. Atmos. Sci.*, **22**, 40-63.

Lacis, A. A., and J. E. Hansen, 1974: A parameterization for the absorption of solar radiation in the earth's atmosphere. *J. Atmos. Sci.*, **32**, 118-133.

Latif, M. T. P. Barnett, M. A. Cane, M. Flugel, N. E. Graham, H. von Storch, J.-S. Xu and S. E. Zebiak, 1994: A Review of ENSO prediction studies. *Climate Dynamics*, **9**, 167-179.

Latif, M., A. Sterl, E. Maier-Reimer, M. M. Junge, 1993a: Climate variability in a coupled GCM. Part I: The tropical Pacific. *J. Climate*, **6**, 5-21.

Latif, M., A. Sterl, E. Maier-Reimer, M. M. Junge, 1993b: Structure and Predictability of the El Niño/Southern Oscillation phenomena in a coupled ocean-atmosphere general circulation model. *J. Climate,* **6**, 700-708.

Latif, M. and A. Villwock, 1990: Interannual variability as simulated in coupled ocean-atmosphere models. *J. Mar. Systems*, **1**, 51-60.

Leetmaa, A. and M. Ji, 1989: Operational hindcasting of the tropical Pacific. *Dyn. Atmos. Oceans*, **13**, 465-490.

Mechoso C. R., A. W. Robertson, N. Barth, M. K. Davey, P. Delecluse, B. Kirtman, M. Latif, T. Nagai, S. G. H. Philander, P. S. Schopf, T. Stockdale, M. J. Suarez, O. Thual, J. Tribbia, 1995: The seasonal cycle over the tropical Pacific in general circulation models. *Mon. Wea. Rev.* (in press).

Mellor, G. L., and T. Yamada, 1982: Development of a turbulence closure model for geophysical fluid problems. *Rev. Geophys. Space Phys.*, **20**, 851-875.

Miyakoda, K. and J. Sirutis, 1977: Comparative integrations of global spectral models with various parameterized processes of sub-grid scale vertical transports. *Beitr. Phys. Atmos.*, **50**, 445-487.

Neelin, J. D., and F.-F. Jin, 1993: Modes of interannual tropical ocean-atmosphere interaction-a unified view. Part II: Analytical results in the weak coupling limit. *J. Atmos. Sci.*, **50**, 3504-3522.

Neelin, J. D., 1990: A hybrid coupled general circulation model for El Niño studies. *J. Atmos. Sci.*, **47**, 674-693.

Oberhuber, J. M., 1988: An atlas based on the COADS data set: the budgets of heat buoyancy and turbulent kinetic energy at the surface of the global ocean, Rep. 15, 199 pp, Max-Planck-Inst. für Meteorol., Hamburg, Germany.

Pacanowski, R. C. and S. G. H. Philander, 1981: Parameterization of the vertical mixing in numerical models of tropical oceans. *J. Phys. Oceanogr.*, **11**, 1443-1451.

Pacanowski, R. C., K. Dixon, A. Rosati, 1993: The GFDL modular ocean model users guide, version 1.0. GFDL Ocean Group Tech. Rep., No. 2.

Palmer, T. N., G. J. Shutts and R. Swinbank, 1986: Alleviation of a systematic westerly bias in general circulation and numerical weather prediction model through an orographic gravity wave parameterization. *Quart. J. Roy. Meteor. Soc.*, **112**, 1001-1039.

Philander, S. G. H., R. C. Pacanowski, N. C. Lau and M. J. Nath, 1992: Simulation of ENSO with a global atmospheric GCM coupled to a high-resolution, tropical Pacific ocean GCM. *J. Climate*, **5**, 308-329.

Philander, S. G. H., 1990: El Niño, La Niña, and the Southern Oscillation. Academic Press, New York, 293 pp.

Philander, S. G. H., and R. C. Pacanowski, 1986: A model of the seasonal cycle in the tropical Atlantic. *J. Geophys. Res.*, **91**, 14192-14206.

Pierrehumbert, R. T., 1987: An essay on the parameterization of orographic gravity wave drag. Geophysics Fluid Dynamics Laboratory/NOAA/Princeton University, 32 pp. [Available from GFDL/NOAA, Princeton University, Princeton, NJ 08542].

Reynolds, R.W., 1988: A real time global sea surface temperature analysis. *J. Climate,* **1,** 75-86.

Rosati, A. and K. Miyakoda, 1988: A general circulation model for upper ocean simulation. *J. Phys. Oceanogr.*, **18**, 1601-1626.

Schneider, E. K., Z. Zhu, B. Huang, B. Giese, B. P. Kirtman and J. Shukla, 1995: ENSO Variability in a coupled general circulation model. *Mon. Wea. Rev.*, (submitted).

Schneider, E. K., B. Huang and J. Shukla, 1995: Ocean wave dynamics and El Niño. *J. Climate,* (in press).

Schneider, E. K. and J. L.Kinter III, 1994: An examination of internally generated variability in long climate simulations. *Climate Dynamics*, **10,** 181-204.

Tiedtke, M., 1984: The effect of penetrative cumulus convection on the large-scale flow in a general circulation model. *Beitr. Phys. Atmos.*, **57**, 216-239.

Trenberth, K. E., W. G. Large and J. G. Olson, 1990: The mean annual cycle in global ocean wind stress. *J. Phys. Oceanogr.*, **20**, 1742-1760.

Xue, Y., P. J. Sellers, J. L. Kinter III, and J. Shukla, 1991: A simple biosphere model for global climate studies. *J. Climate*, **4**, 345-364.

Zebiak, S. E. and M. A. Cane, 1987: A model of El Niño and the southern oscillation. *Mon. Wea. Rev.*, **115**, 2262-2278.

Zhu, Z., and E. K. Schneider, 1995: Experimental multi-season ENSO predictions with an anomaly coupled general circulation model. COLA Technical Report No. 10. 18 pp.

Figure Captions

Figure 1: Time-longitude cross section of the zonal wind stress annual cycle along the equator: (a) FSU annual cycle, (b) AGCM surface wind stress annual cycle and (c) difference between AGCM and FSU data. Contour interval 0.1 dynes cm^{-2}.

Figure 2: Time-longitude cross section of the SST annual cycle along the equator: (a) Reynolds observed annual cycle, (b) OGCM annual cycle with FSU forcing and (c) difference between OGCM and observed data.

Figure 3: Time-longitude cross section of the zonal wind stress anomaly along the equator: (a) AGCM surface stress, (b) FSU data and (c) AGCM zonal wind converted to zonal surface stress. Contour interval 0.1 dynes cm^{-2}.

Figure 4: Composite wind stress anomaly vectors (DJF 82-83, 87-88 and 91-92): (a) AGCM surface stress, (b) FSU data and (c) AGCM zonal wind converted to zonal surface stress.

Figure 5: Time-longitude cross section of SSTA along the equator: (a) OGCM forced by AGCM wind stress, (b) OGCM forced by FSU wind stress, (c) OGCM forced by AGCM 850 mb zonal wind converted into zonal surface stress and (d) Reynolds analysis.

Figure 6: Composite SSTA (DJF 82-83, 87-88 and 91-92): (a) OGCM forced by AGCM surface stress, (b) OGCM forced by FSU data, (c) OGCM forced AGCM zonal wind converted to zonal surface stress and (d) Reynolds analysis.

Figure 7: Time-longitude cross section of the zonal wind stress anomaly along the equator: (a) AGCM zonal wind converted to zonal surface stress and (b) after one iteration of the zonal wind stress assimilation. Contour interval 0.1 dynes cm^{-2}.

Figure 8: Time-longitude cross section of SSTA along the equator: (a) OGCM forced by AGCM 850 mb zonal wind converted into zonal surface stress, (b) Reynolds analysis and (c) after one iteration of the zonal wind stress assimilation.

Figure 9: Temporal correlation of the observed SSTA and the simulated SSTA (a) After the iterative wind stress assimilation and (b) before the wind stress assimilation.

Figure 10: Evolution of the NINO3 SSTA systematic error. Open circles denotes the forecasts initialized in January and the closed circles gives the forecasts initialized in July.

Figure 11: Horizontal structure of the systematic error. (a) Forecasts initialized in January for lead times of 10 months and (b) forecasts initialized in July with lead times of 8 months.

Figure 12: Evolution of NINO3 SSTA for all 30 forecasts and the observed SSTA. The thin curves denote the forecasts and the thick curves is for the observed SSTA.

Figure 13: NINO3 correlation coefficient and RMSE. The curves marked ZC1 and ZC2 are for the Zebiak-Cane model without and with the initialization procedure respectively (see Chen et al., 1995). The curves marked CMP1 and CMP2 are for the NMC coupled model project before and after the statistical correction was applied to the wind stress (Ji et al., 1994a and Ji et al., 1995). The curves marked COLA1, COLA2 and COLA3 denote various versions of the prediction model presented here (see text for details) and the most recent version is COLA3.

Figure 14: Horizontal structure of the (a) observed and (b) predicted SSTA warm composite (DJF 65-66, DJF 72-73, DJF 82-83, DJF 87-88).

Figure 15: Horizontal structure of the (a) observed and (b) predicted SSTA cold composite (DJF 70-71, DJF 73-74, DJF 84-85, DJF 88-89).

Figure 16: Horizontal structure of the (a) assimilated and (b) predicted zonal wind stress anomaly warm composite (DJF 65-66, DJF 72-73, DJF 82-83, DJF 87-88).

Figure 17: Horizontal structure of the (a) assimilated and (b) predicted zonal wind stress anomaly cold composite (DJF 70-71, DJF 73-74, DJF 84-85, DJF 88-89).

Figure 18: Horizontal structure of the (a) AGCM uncoupled simulation with observed SST and (b) predicted sea level pressure anomaly warm composite (DJF 65-66, DJF 72-73, DJF 82-83, DJF 87-88).

Figure 19: Horizontal structure of the (a) AGCM uncoupled simulation with observed SST and (b) predicted sea level pressure anomaly cold composite (DJF 70-71, DJF 73-74, DJF 84-85, DJF 88-89).

Figure 20: Horizontal structure of the (a) AGCM uncoupled simulation with observed SST and (b) predicted precipitation anomaly warm composite (DJF 65-66, DJF 72-73, DJF 82-83, DJF 87-88).

Figure 21: Horizontal structure of the (a) AGCM uncoupled simulation with observed SST and (b) predicted precipitation anomaly cold composite (DJF 70-71, DJF 73-74, DJF 84-85, DJF 88-89).

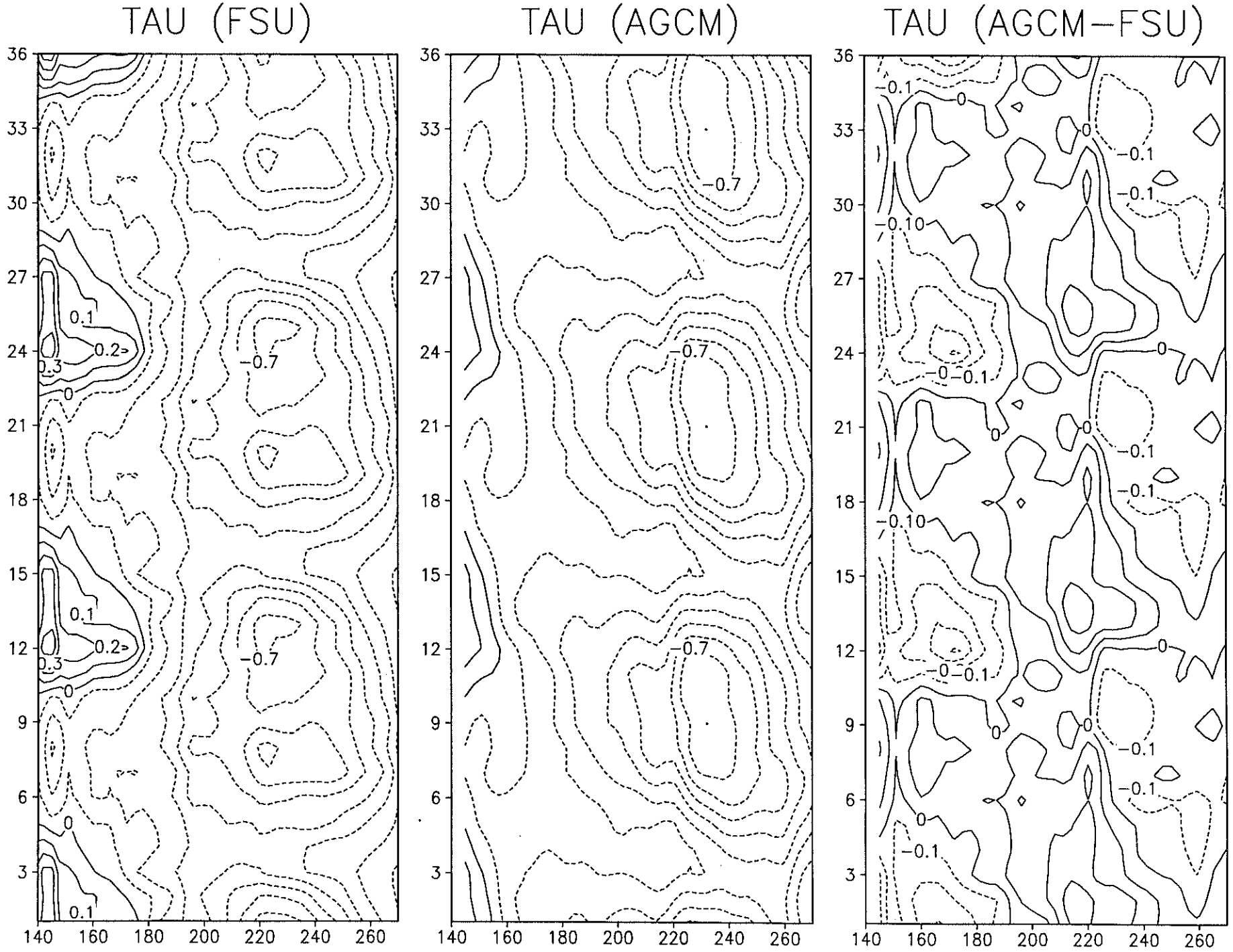
TAU (FSU)
TAU (AGCM)
TAU (AGCM−FSU)
36
33
30
27
24
21
18
15
12
9
6
3
140
160
180
200
220
240
260
0.1
0.2
0.3
0
−0.7
−0.1
−0.10

Figure 1

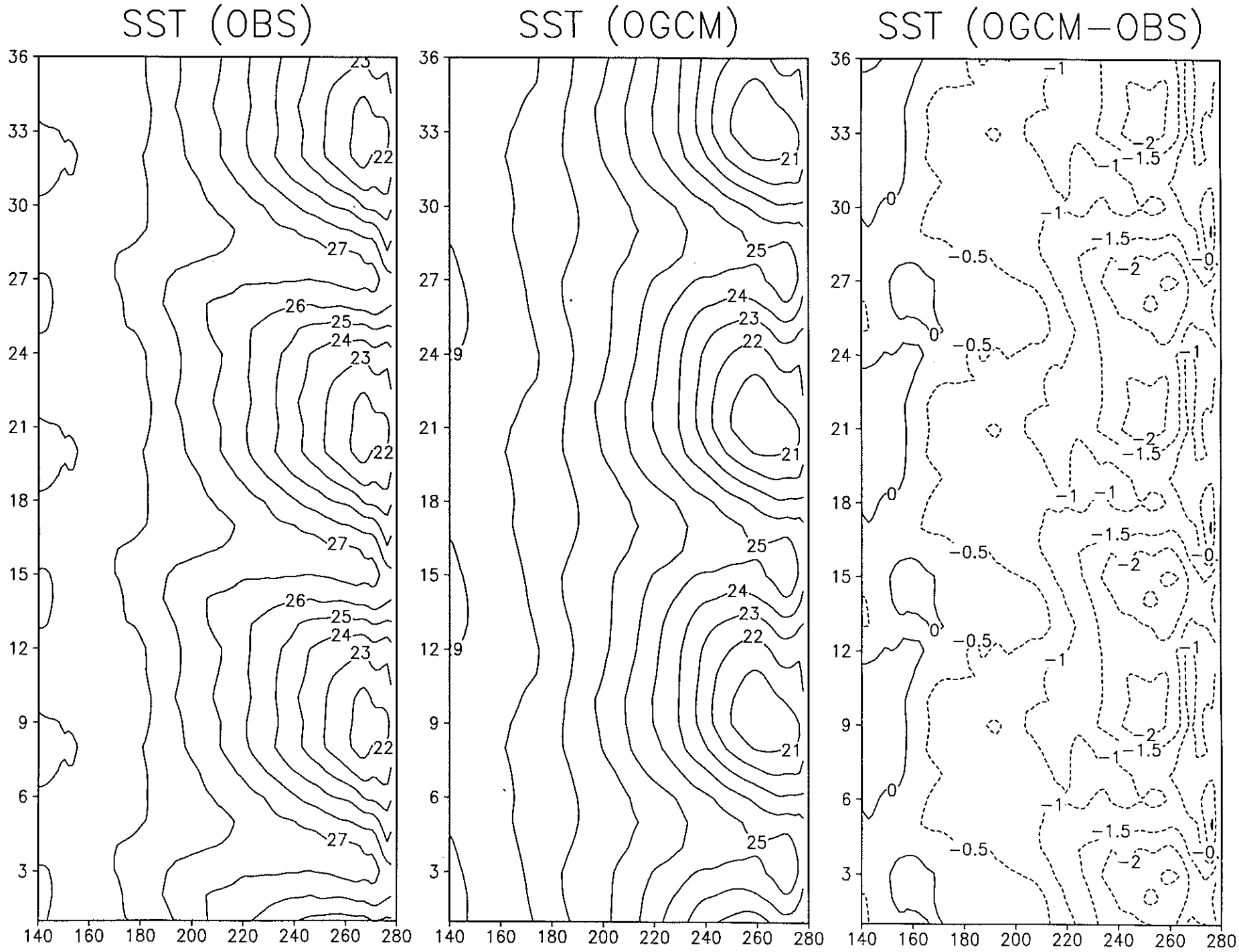
SST (OBS)
SST (OGCM)
SST (OGCM−OBS)
36
33
30
27
24
21
18
15
12
9
6
3
140
160
180
200
220
240
260
280
23
22
27
26
25
24
23
22
27
26
25
24
23
22
27
21
25
24
23
22
21
25
24
23
22
21
25
9
9
−1
−2
−1.5
−1
−1
−1.5
−2
−0
0
−0.5
0
−0.5
−1
−2
−1.5
−1
−1
−1.5
−2
−0
0
−0.5
−1
−2
−1.5
−1
−1
−1.5
−2
−0
0
−0.5

Figure 2

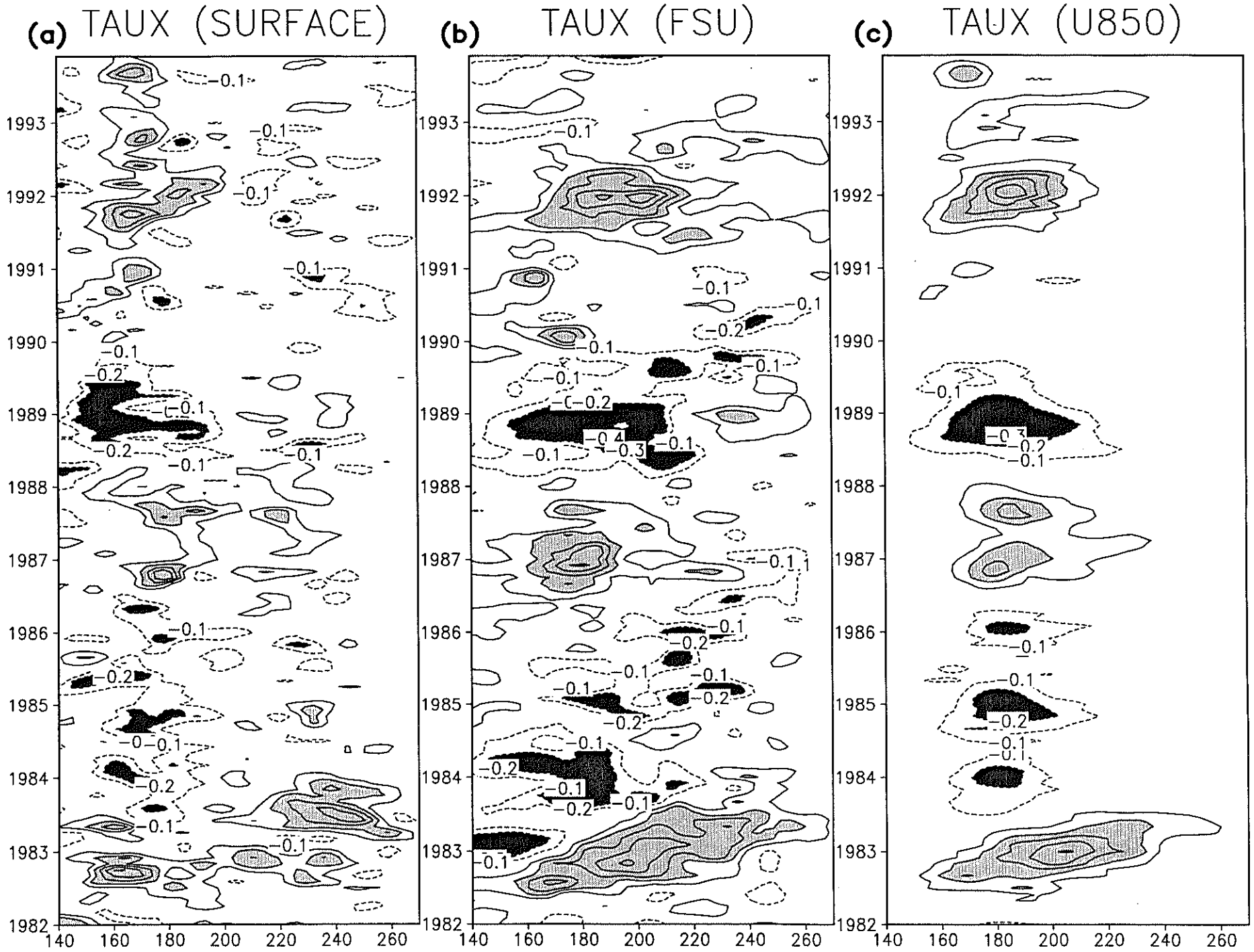
(a) TAUX (SURFACE)
(b) TAUX (FSU)
(c) TAUX (U850)
1993
1992
1991
1990
1989
1988
1987
1986
1985
1984
1983
1982
140
160
180
200
220
240
260

Figure 3

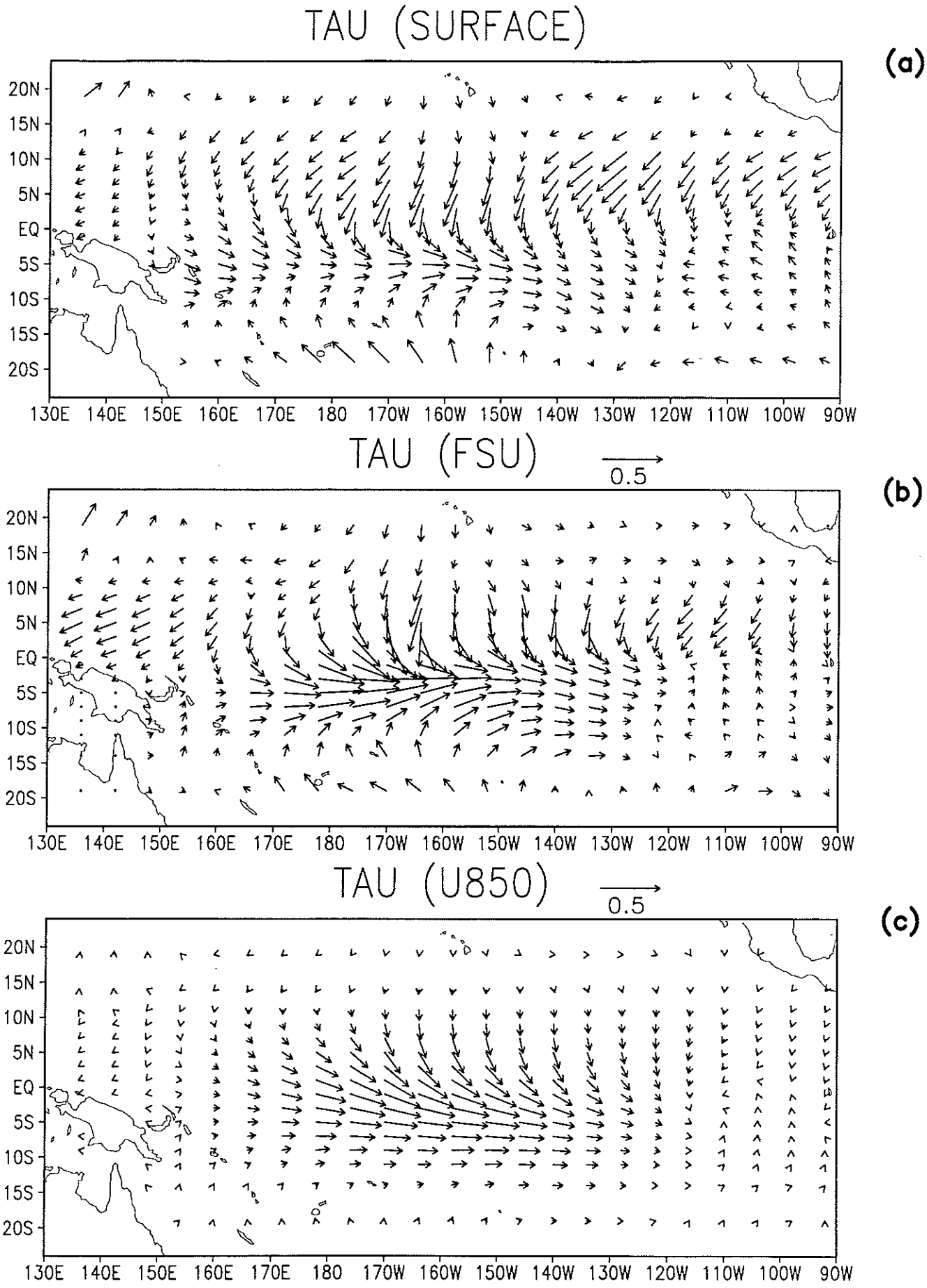
TAU (SURFACE)
(a)
20N
15N
10N
5N
EQ
5S
10S
15S
20S
130E 140E 150E 160E 170E 180 170W 160W 150W 140W 130W 120W 110W 100W 90W
TAU (FSU)
0.5
(b)
20N
15N
10N
5N
EQ
5S
10S
15S
20S
130E 140E 150E 160E 170E 180 170W 160W 150W 140W 130W 120W 110W 100W 90W
TAU (U850)
0.5
(c)
20N
15N
10N
5N
EQ
5S
10S
15S
20S
130E 140E 150E 160E 170E 180 170W 160W 150W 140W 130W 120W 110W 100W 90W
0.5

Figure 4

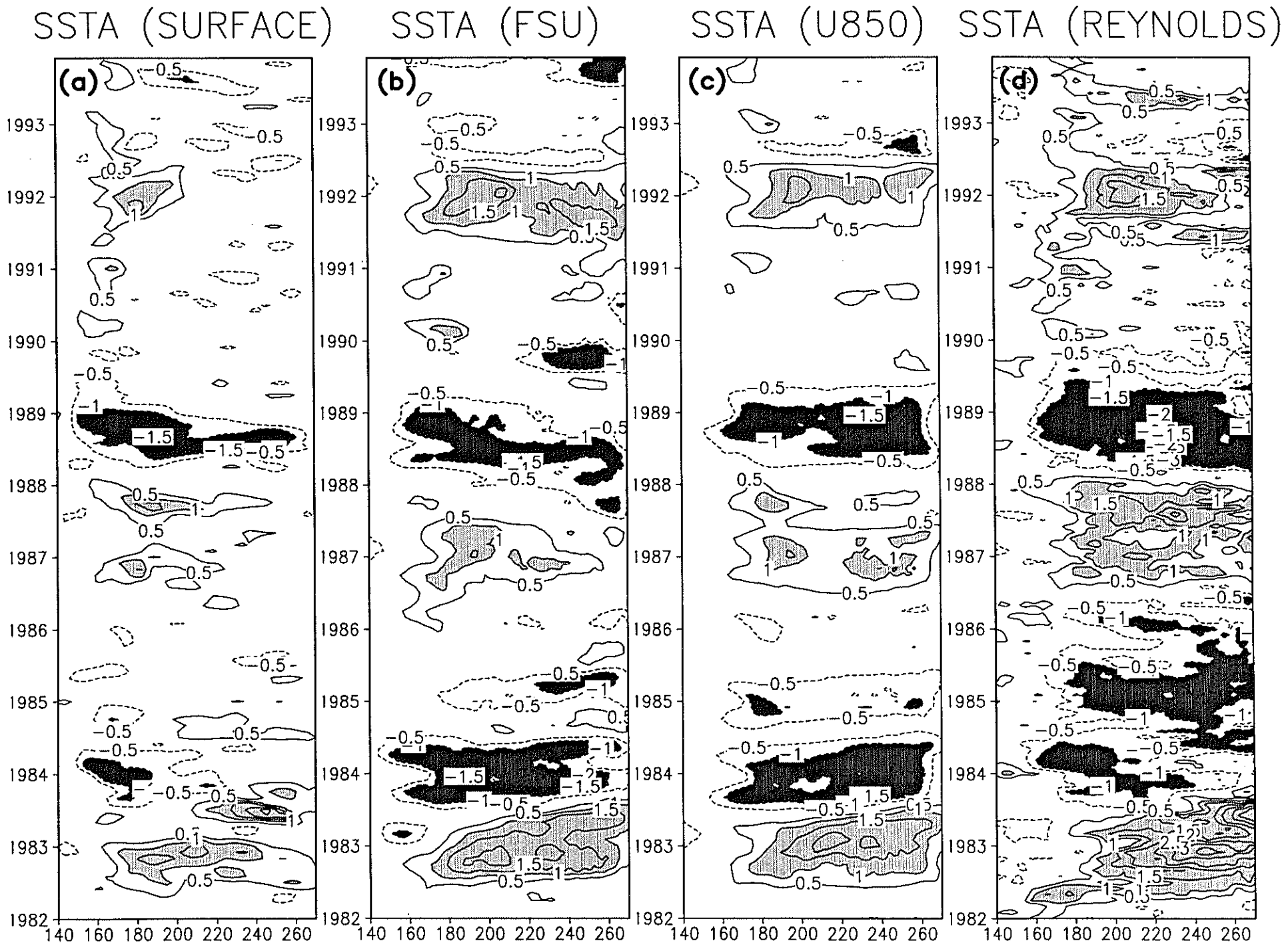
SSTA (SURFACE)
SSTA (FSU)
SSTA (U850)
SSTA (REYNOLDS)
(a)
(b)
(c)
(d)
1993
1992
1991
1990
1989
1988
1987
1986
1985
1984
1983
1982
140 160 180 200 220 240 260

Figure 5

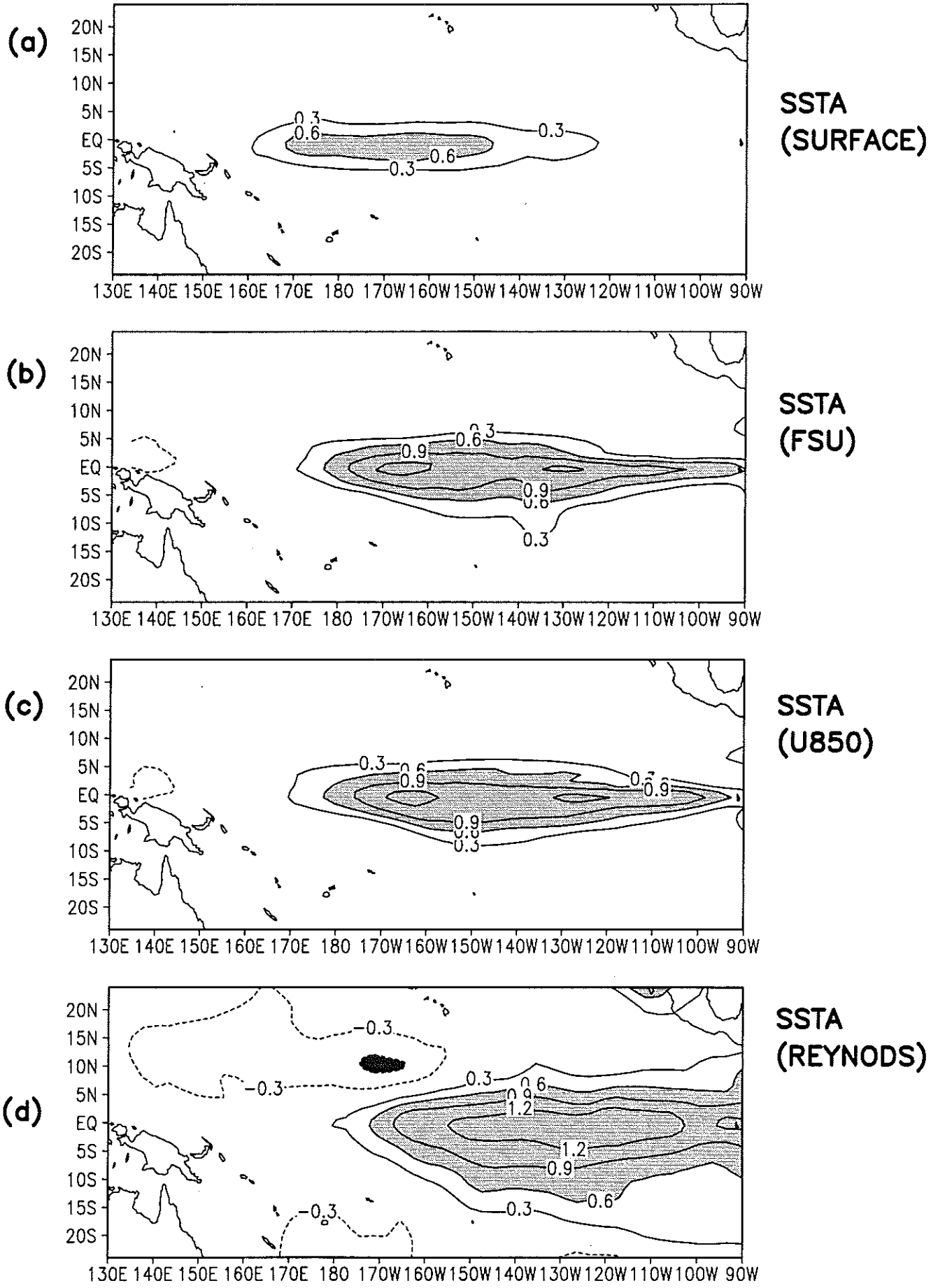
(a)
SSTA
(SURFACE)
(b)
SSTA
(FSU)
(c)
SSTA
(U850)
(d)
SSTA
(REYNODS)
20N
15N
10N
5N
EQ
5S
10S
15S
20S
130E 140E 150E 160E 170E 180 170W 160W 150W 140W 130W 120W 110W 100W 90W

Figure 6

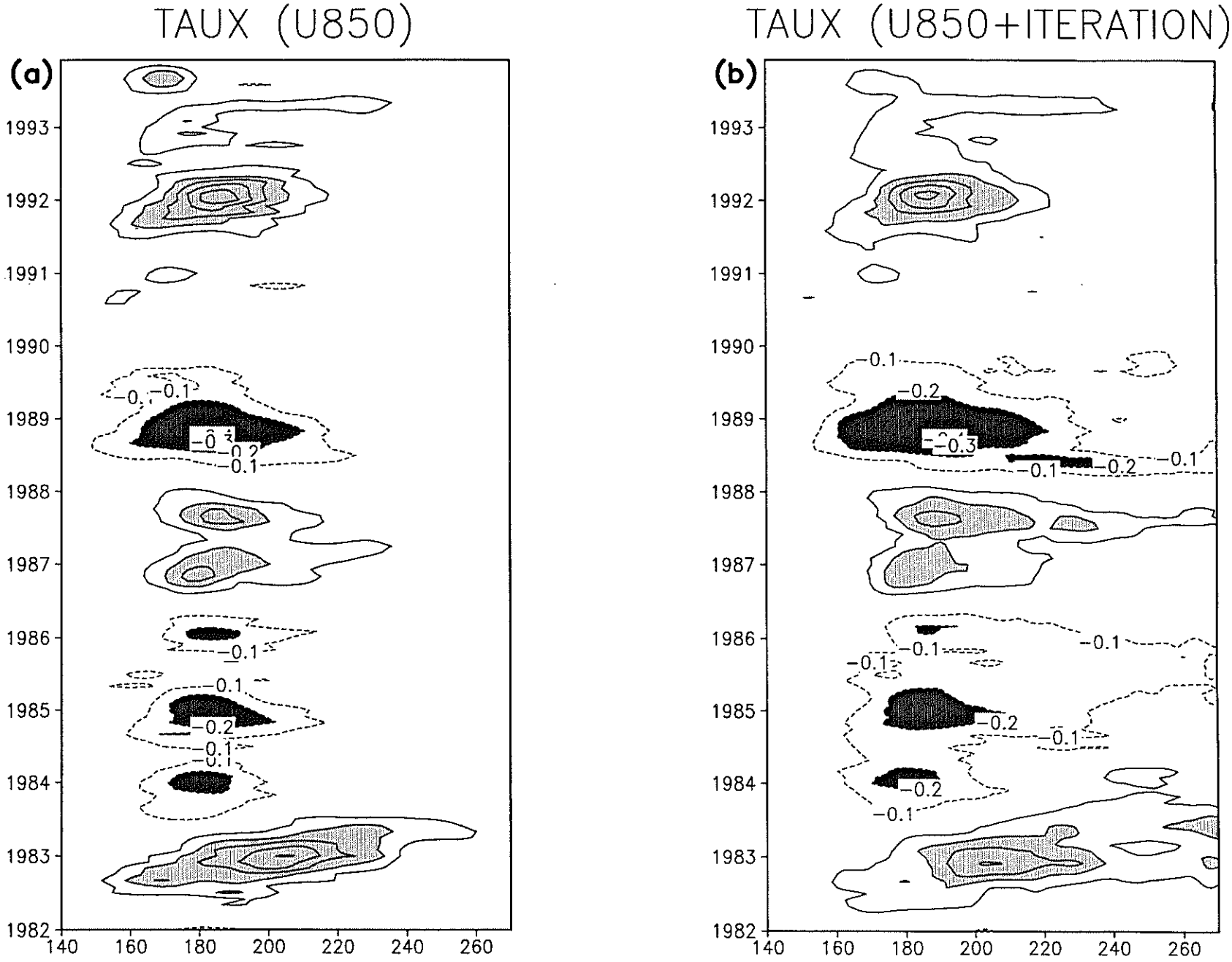
TAUX (U850)
(a)
TAUX (U850+ITERATION)
(b)
1993
1992
1991
1990
1989
1988
1987
1986
1985
1984
1983
1982
140
160
180
200
220
240
260
-0.1
-0.2
-0.3

Figure 7

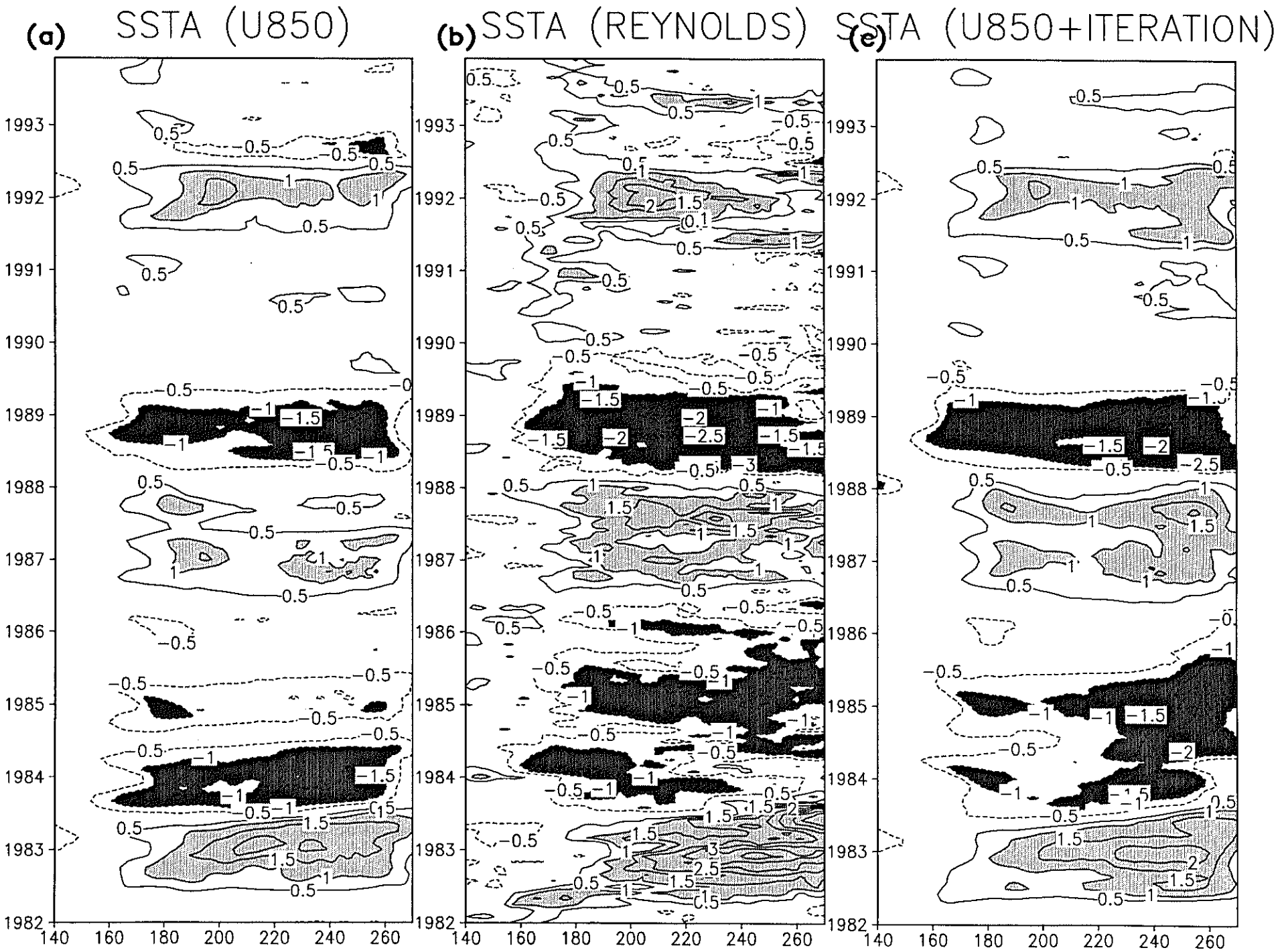
(a) SSTA (U850)
(b) SSTA (REYNOLDS)
(c) SSTA (U850+ITERATION)
1993
1992
1991
1990
1989
1988
1987
1986
1985
1984
1983
1982
140
160
180
200
220
240
260

Figure 8

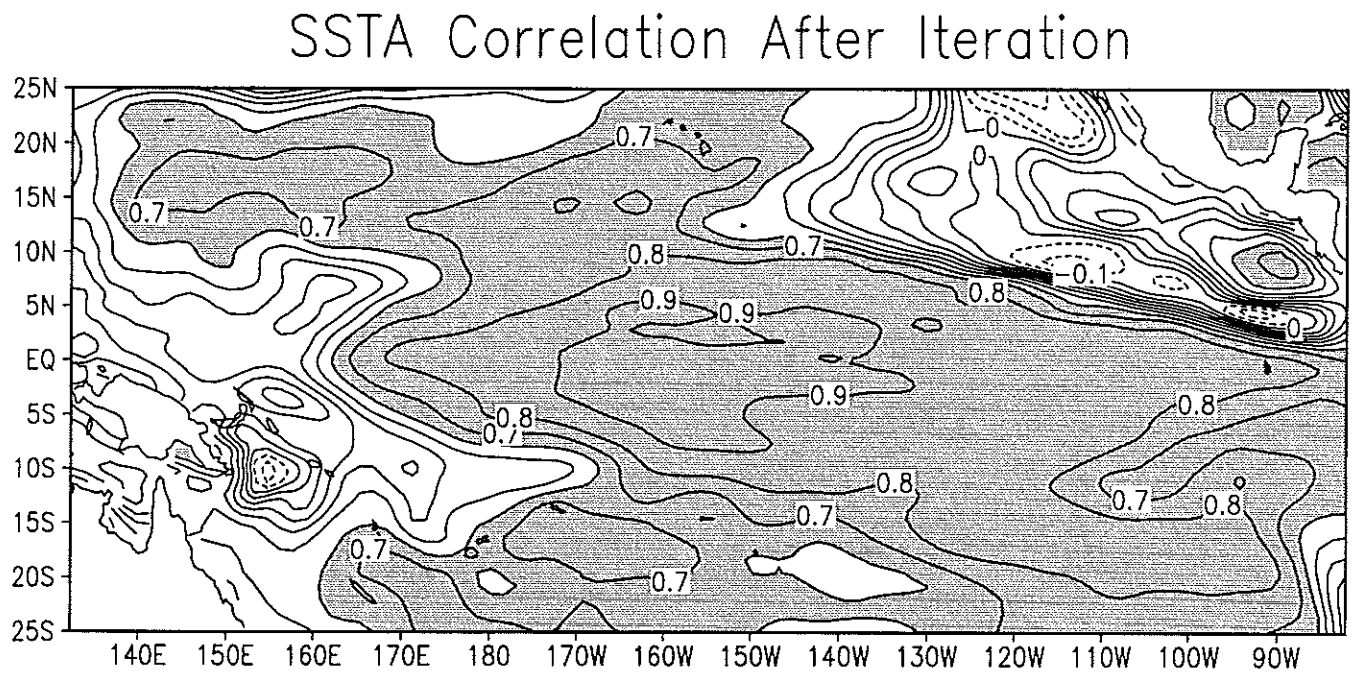
SSTA Correlation After Iteration
25N
20N
15N
10N
5N
EQ
5S
10S
15S
20S
25S
140E
150E
160E
170E
180
170W
160W
150W
140W
130W
120W
110W
100W
90W

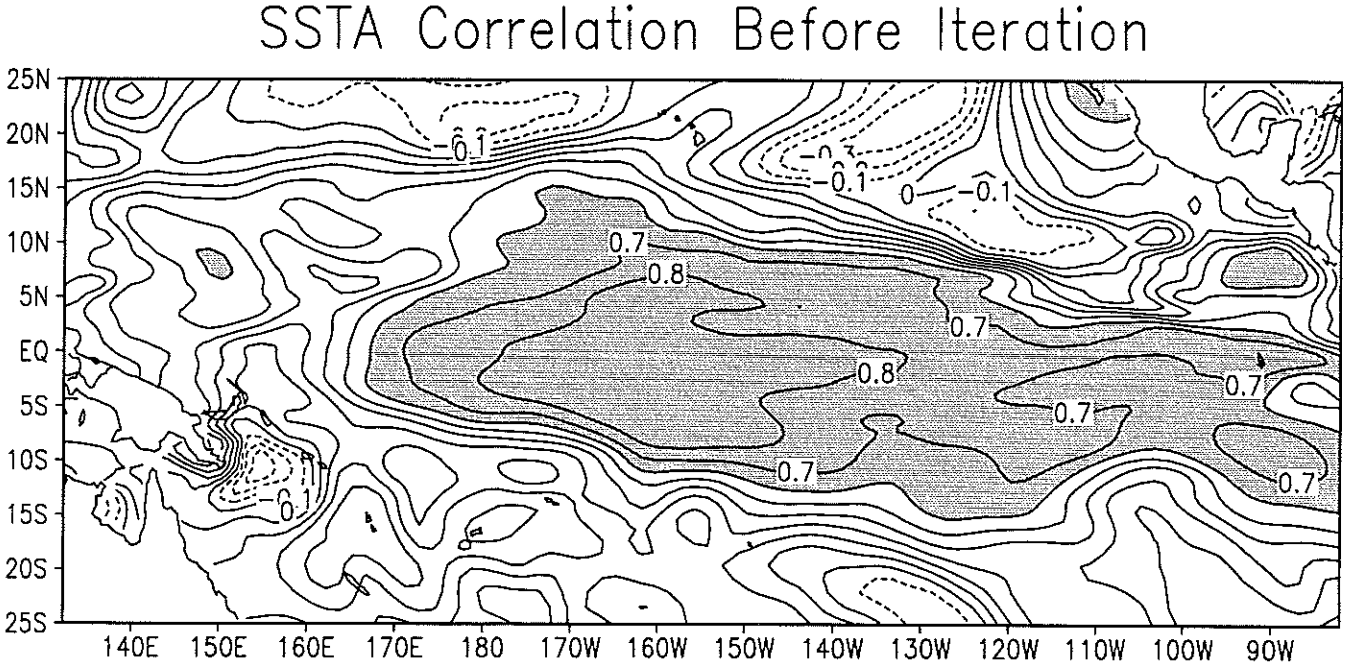
SSTA Correlation Before Iteration
25N
20N
15N
10N
5N
EQ
5S
10S
15S
20S
25S
140E
150E
160E
170E
180
170W
160W
150W
140W
130W
120W
110W
100W
90W

Figure 9

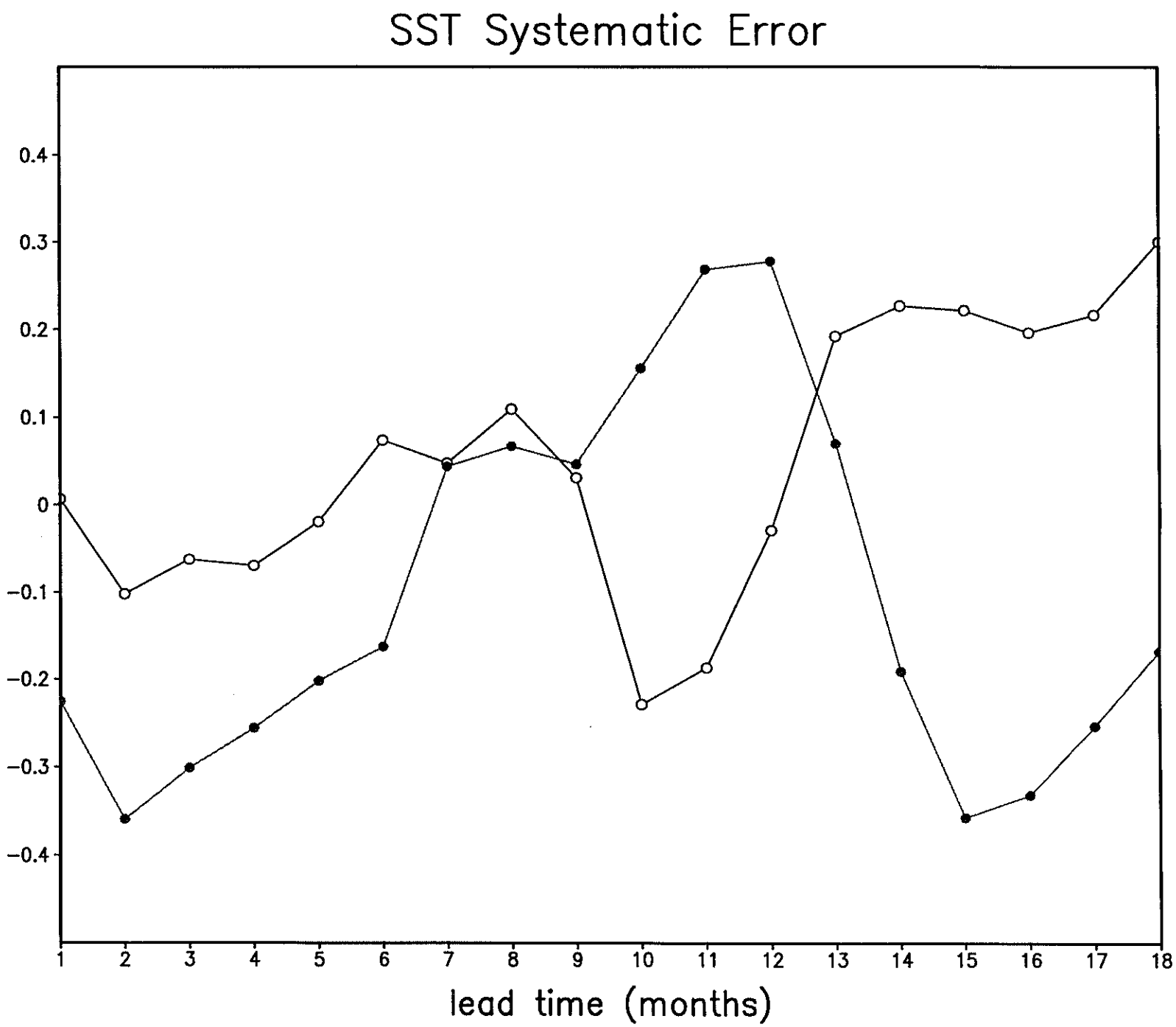
SST Systematic Error
0.4
0.3
0.2
0.1
0
−0.1
−0.2
−0.3
−0.4
1
2
3
4
5
6
7
8
9
10
11
12
13
14
15
16
17
18
lead time (months)

Figure 10

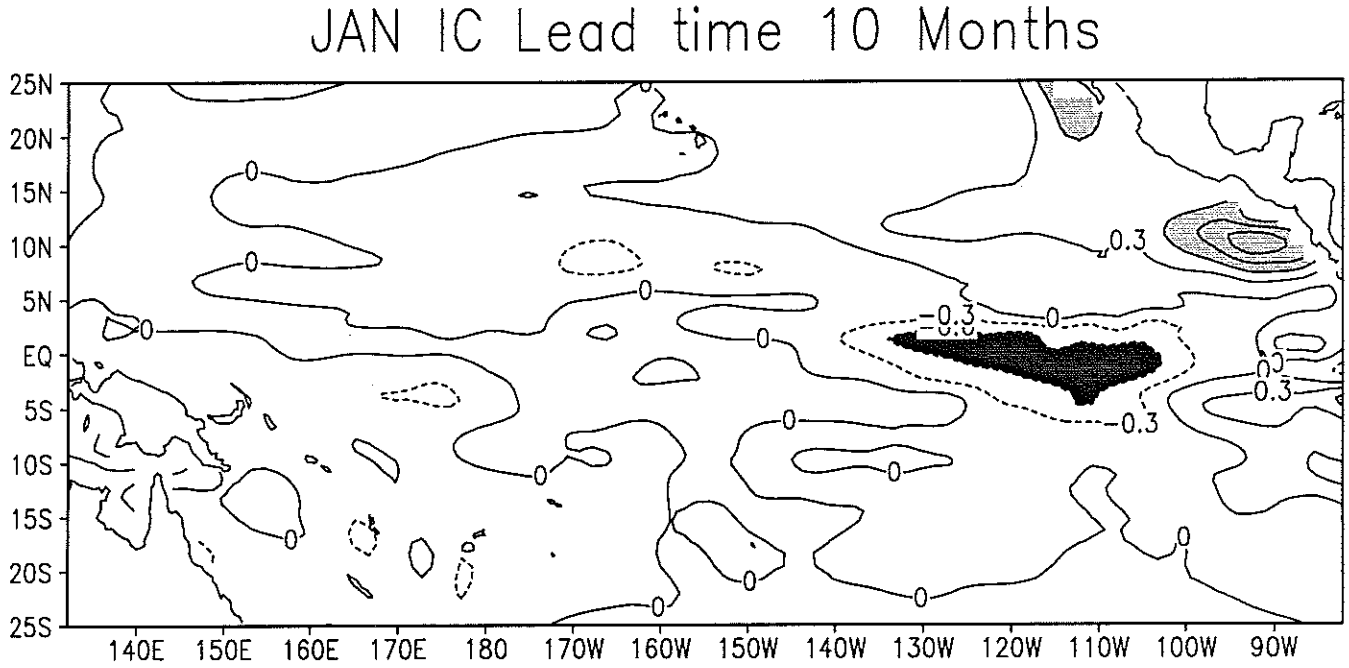
JAN IC Lead time 10 Months
25N
20N
15N
10N
5N
EQ
5S
10S
15S
20S
25S
140E
150E
160E
170E
180
170W
160W
150W
140W
130W
120W
110W
100W
90W

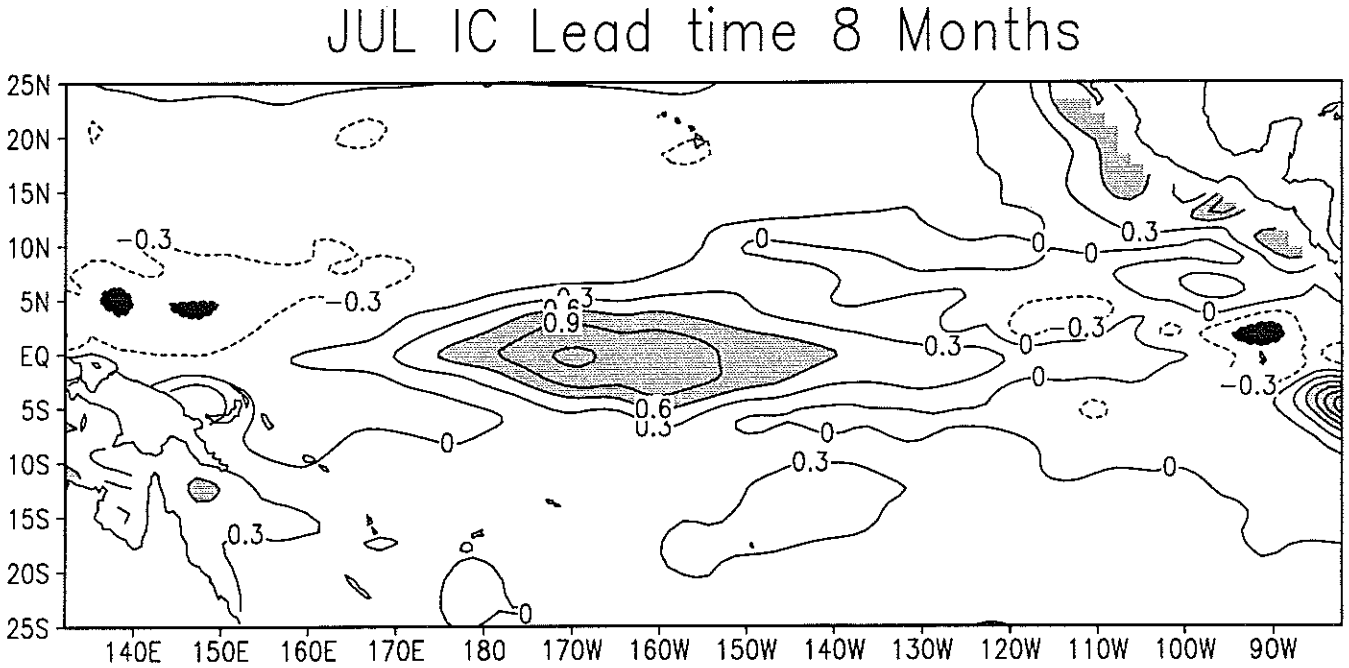
JUL IC Lead time 8 Months
25N
20N
15N
10N
5N
EQ
5S
10S
15S
20S
25S
140E
150E
160E
170E
180
170W
160W
150W
140W
130W
120W
110W
100W
90W

Figure 11

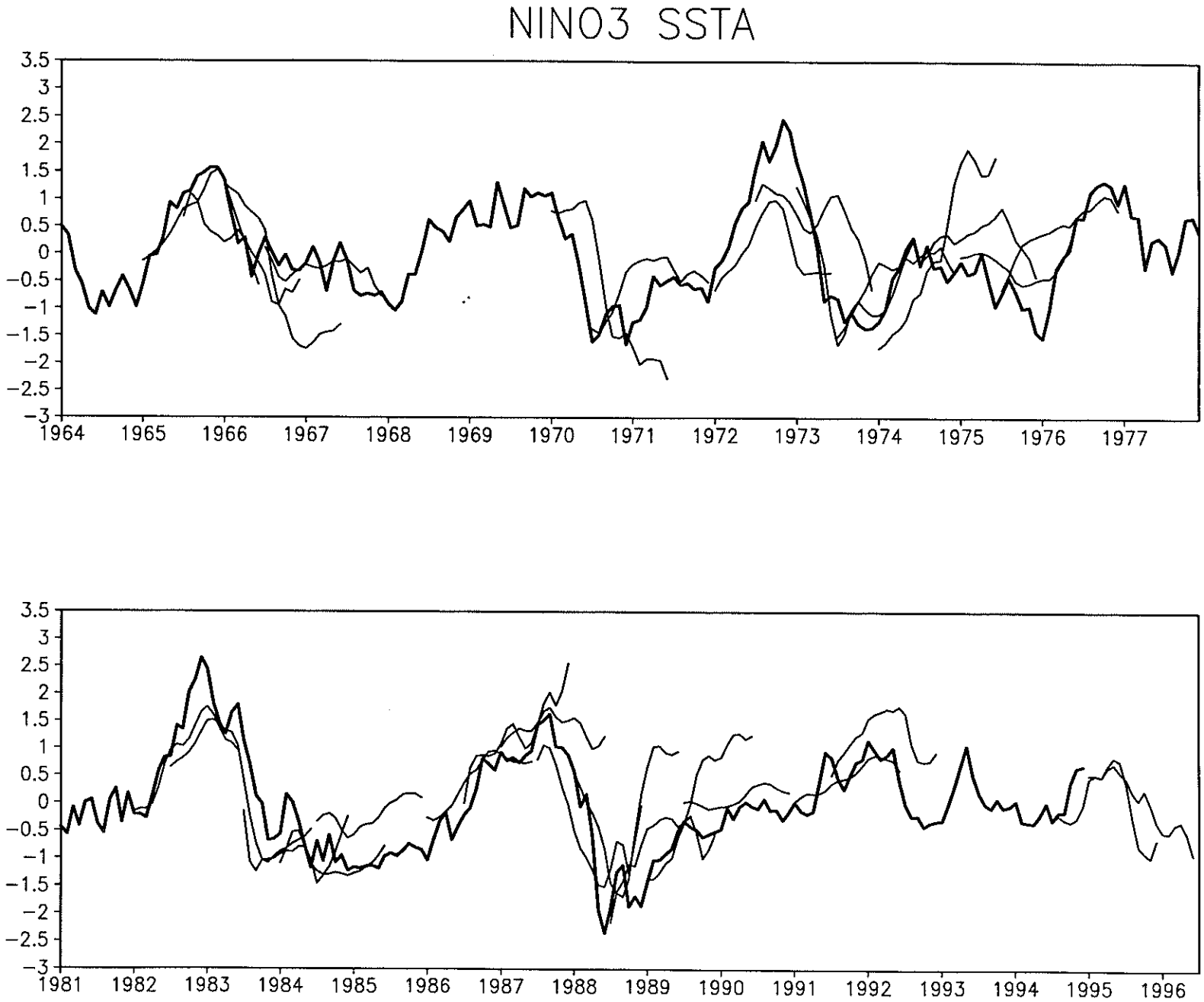
NINO3 SSTA
3.5
3
2.5
2
1.5
1
0.5
0
−0.5
−1
−1.5
−2
−2.5
−3
1964
1965
1966
1967
1968
1969
1970
1971
1972
1973
1974
1975
1976
1977
1981
1982
1983
1984
1985
1986
1987
1988
1989
1990
1991
1992
1993
1994
1995
1996

Figure 12

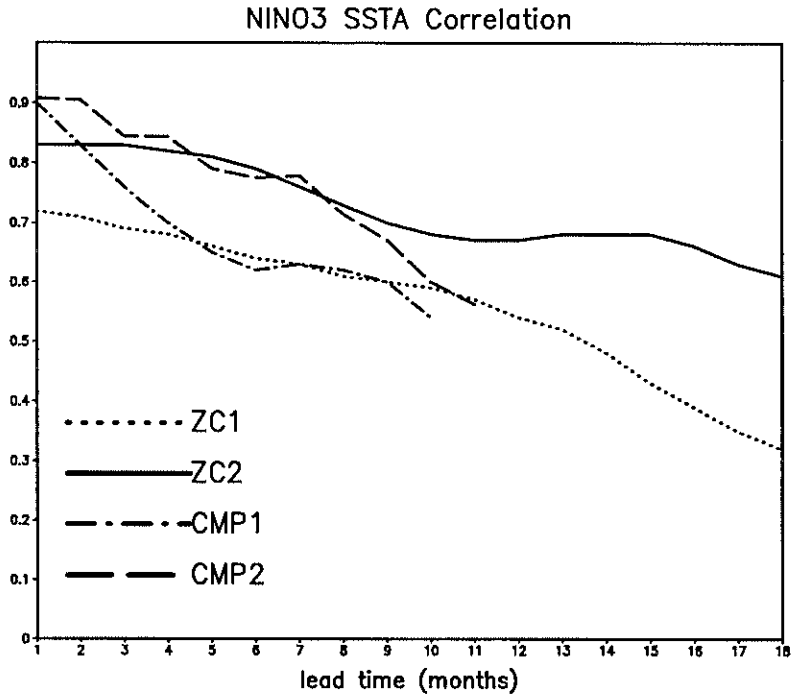
NINO3 SSTA Correlation
ZC1
ZC2
CMP1
CMP2
lead time (months)

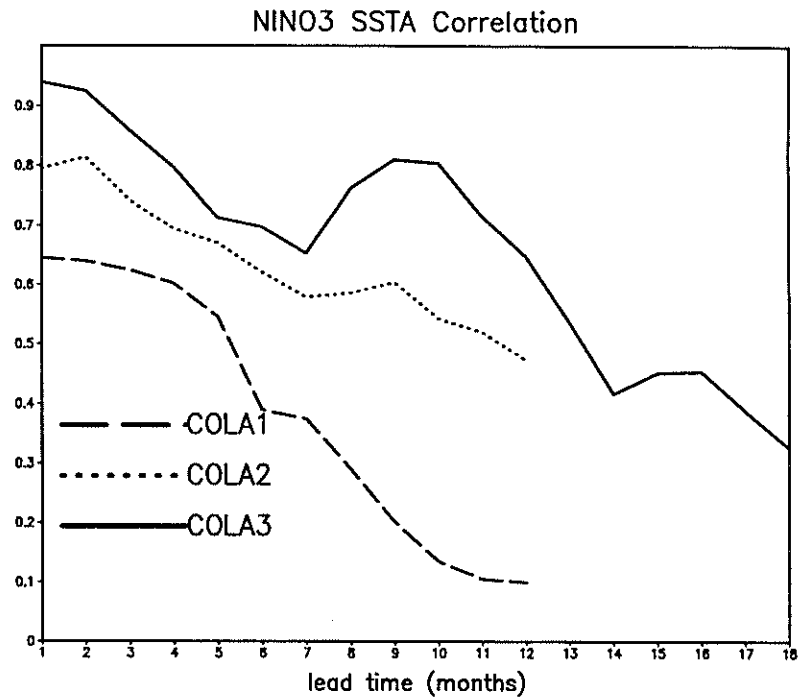
NINO3 SSTA Correlation
COLA1
COLA2
COLA3
lead time (months)

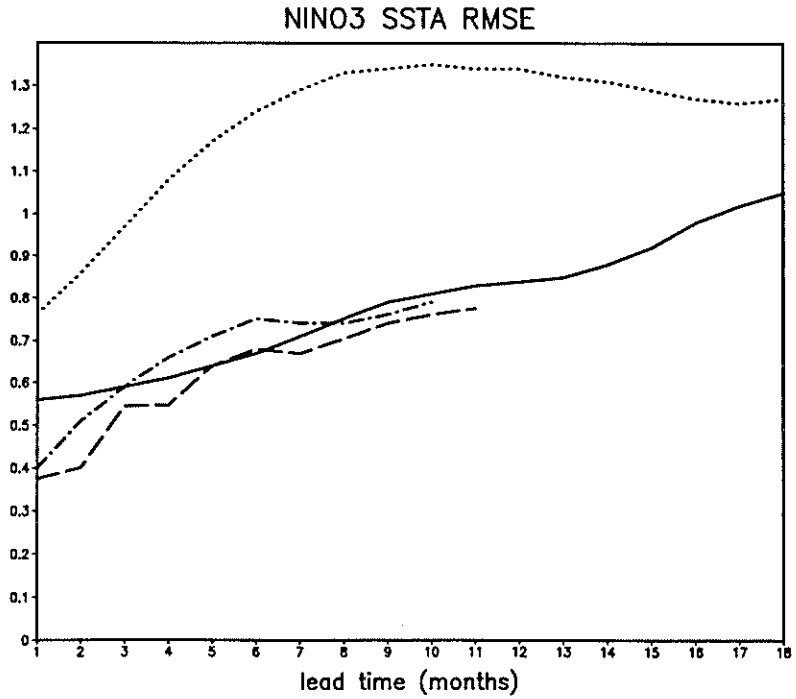
NINO3 SSTA RMSE
lead time (months)

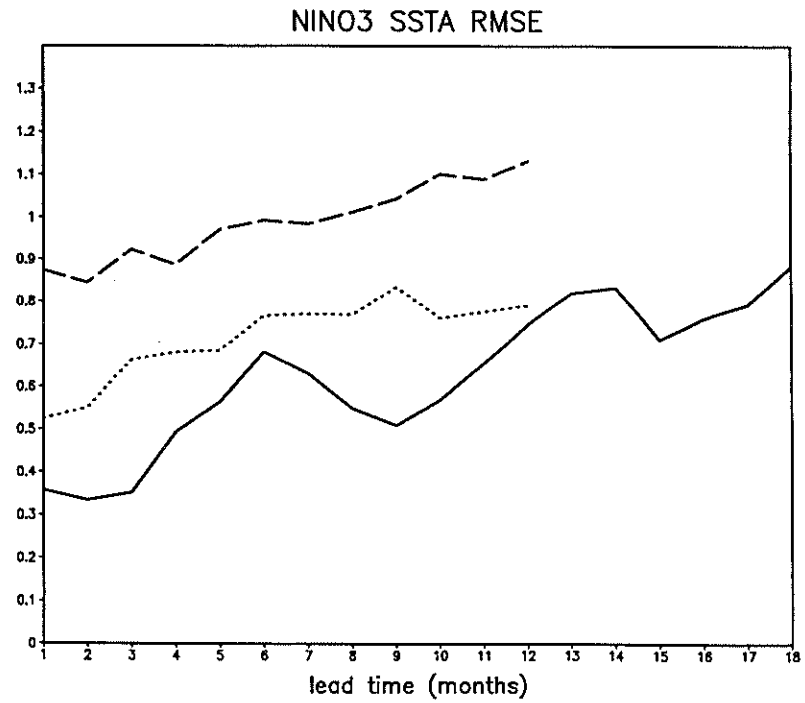
NINO3 SSTA RMSE
lead time (months)

Figure 13

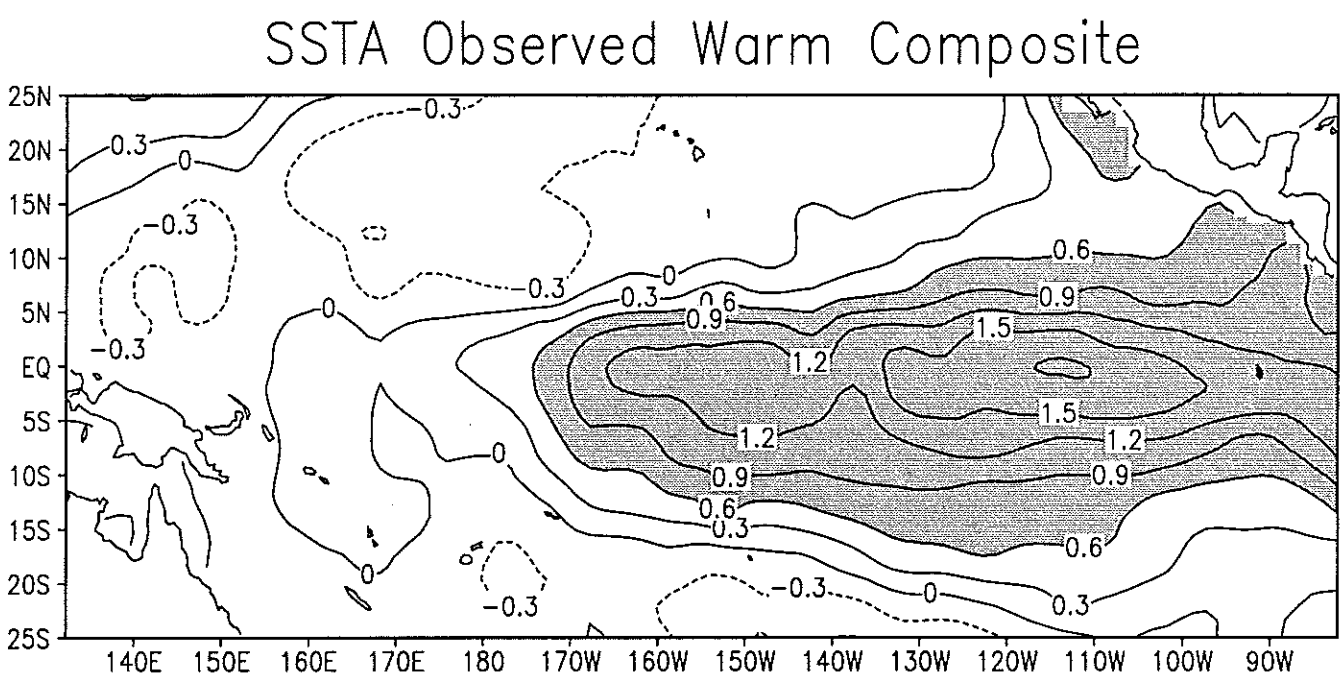
SSTA Observed Warm Composite
25N
20N
15N
10N
5N
EQ
5S
10S
15S
20S
25S
140E
150E
160E
170E
180
170W
160W
150W
140W
130W
120W
110W
100W
90W

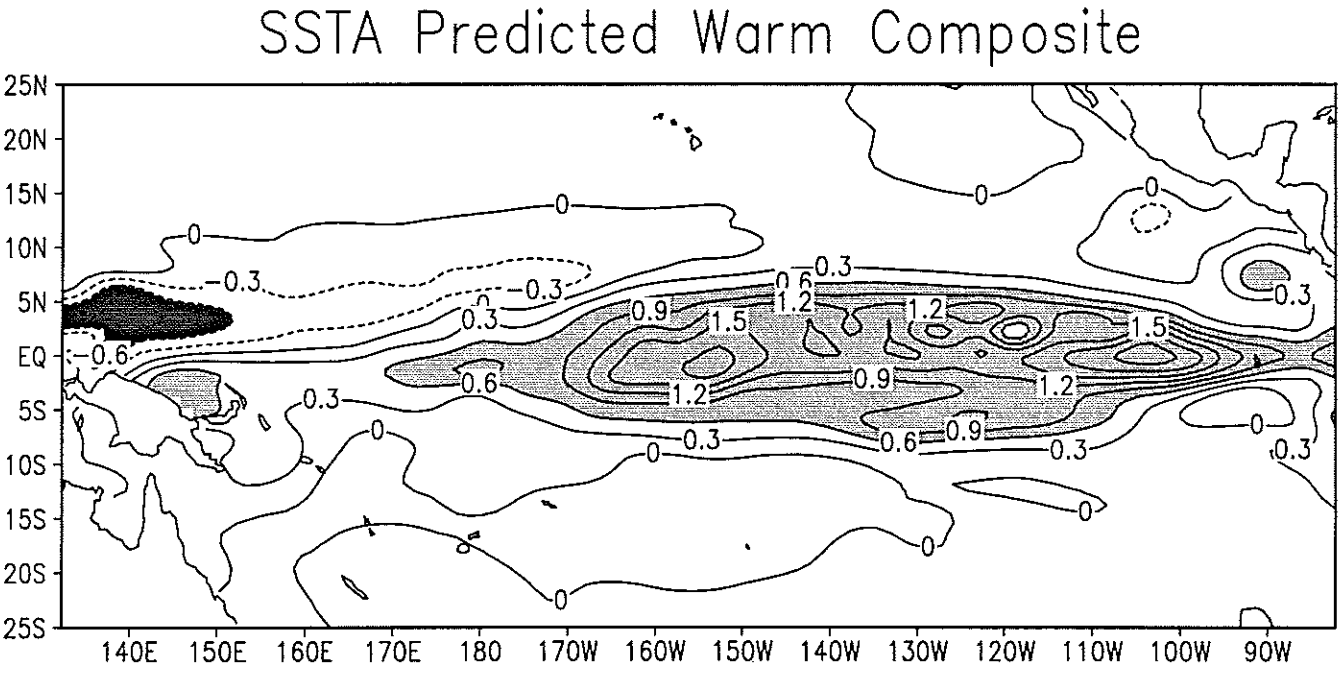
SSTA Predicted Warm Composite
25N
20N
15N
10N
5N
EQ
5S
10S
15S
20S
25S
140E
150E
160E
170E
180
170W
160W
150W
140W
130W
120W
110W
100W
90W

Figure 14

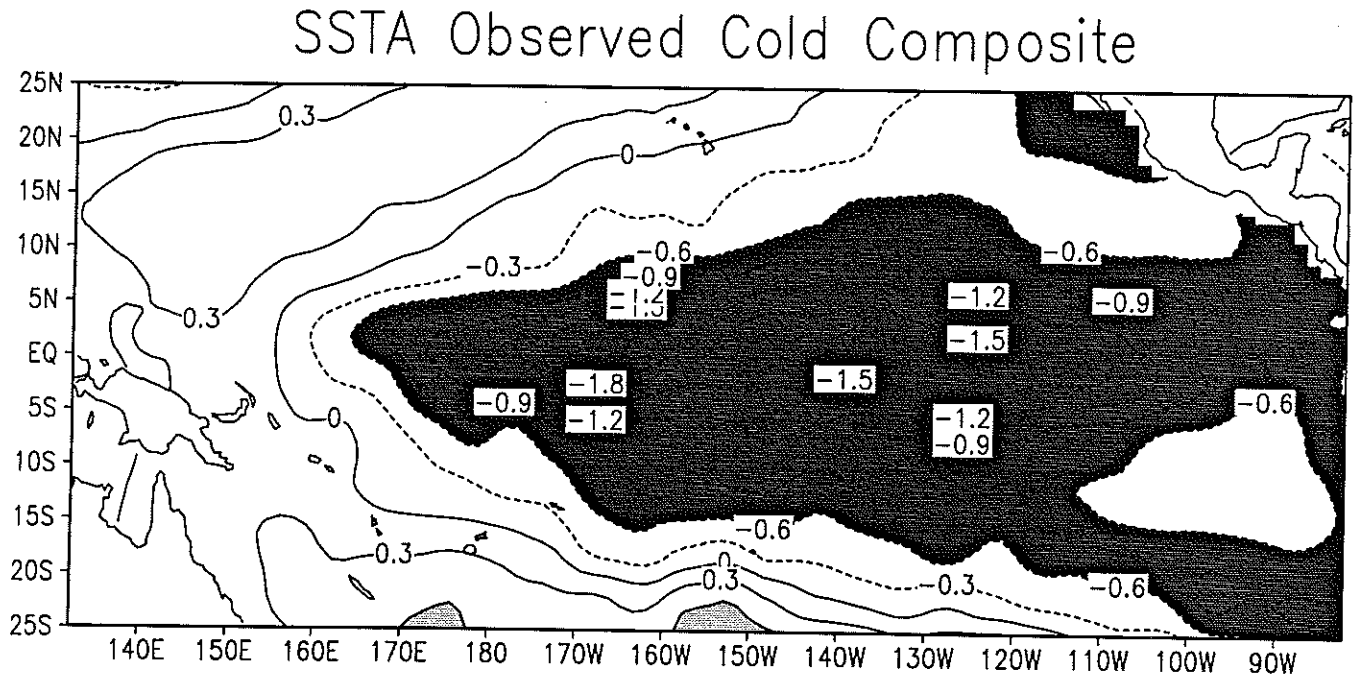
SSTA Observed Cold Composite
25N
20N
15N
10N
5N
EQ
5S
10S
15S
20S
25S
140E 150E 160E 170E 180 170W 160W 150W 140W 130W 120W 110W 100W 90W
0.3
0
-0.3
-0.6
-0.9
-1.2
-1.5
-1.8

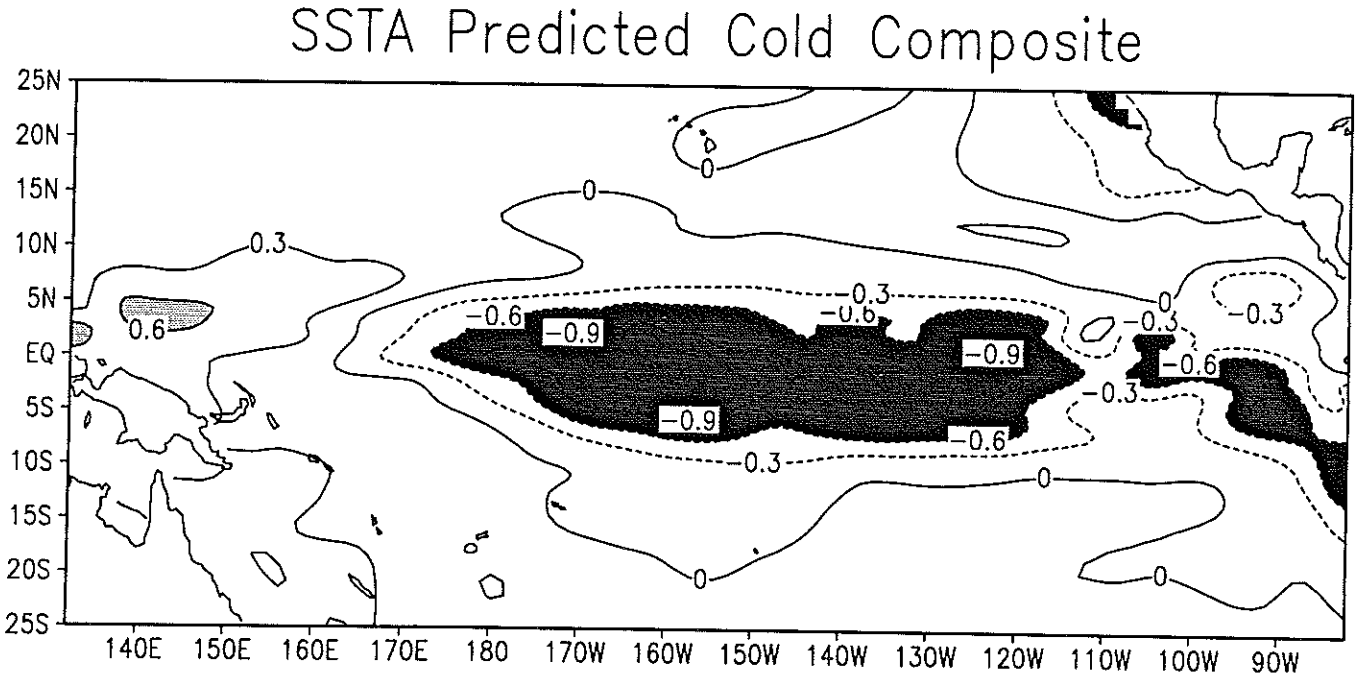
SSTA Predicted Cold Composite
25N
20N
15N
10N
5N
EQ
5S
10S
15S
20S
25S
140E 150E 160E 170E 180 170W 160W 150W 140W 130W 120W 110W 100W 90W
0.6
0.3
0
-0.3
-0.6
-0.9

Figure 15

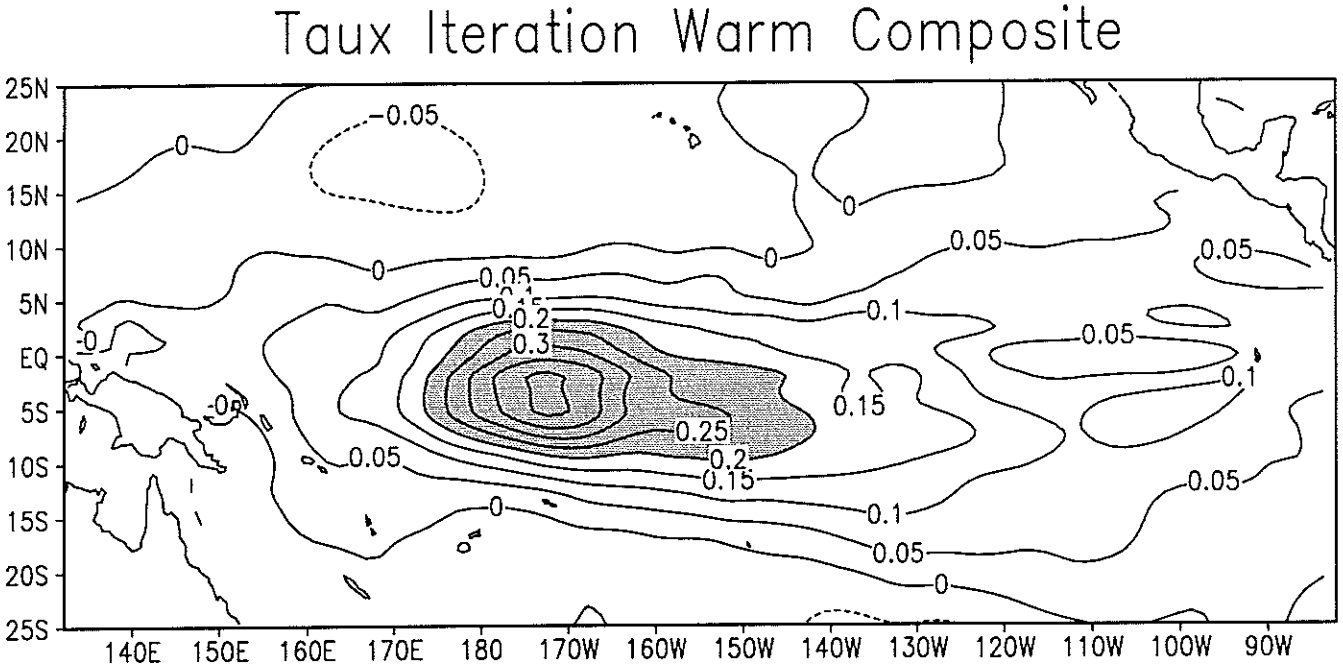
Taux Iteration Warm Composite
25N
20N
15N
10N
5N
EQ
5S
10S
15S
20S
25S
140E
150E
160E
170E
180
170W
160W
150W
140W
130W
120W
110W
100W
90W
-0.05
0
0.05
0.1
0.15
0.2
0.25
0.3

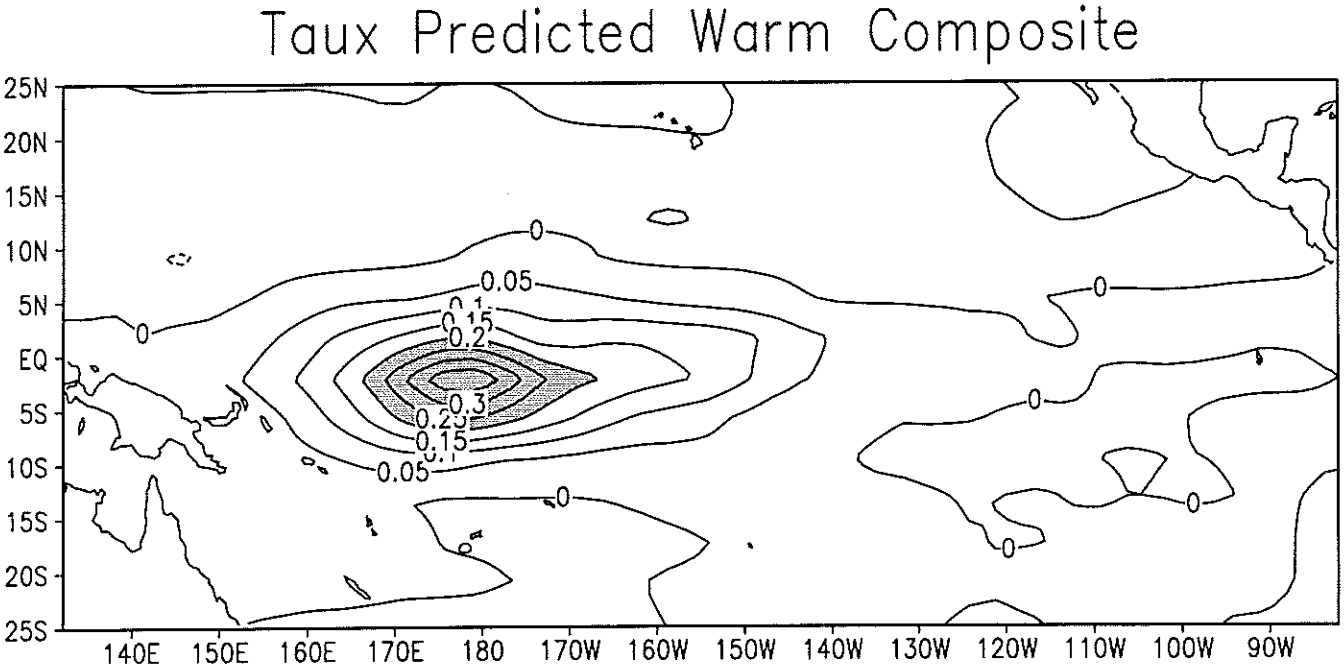
Taux Predicted Warm Composite
25N
20N
15N
10N
5N
EQ
5S
10S
15S
20S
25S
140E
150E
160E
170E
180
170W
160W
150W
140W
130W
120W
110W
100W
90W
0
0.05
0.1
0.15
0.2
0.3

Figure 16

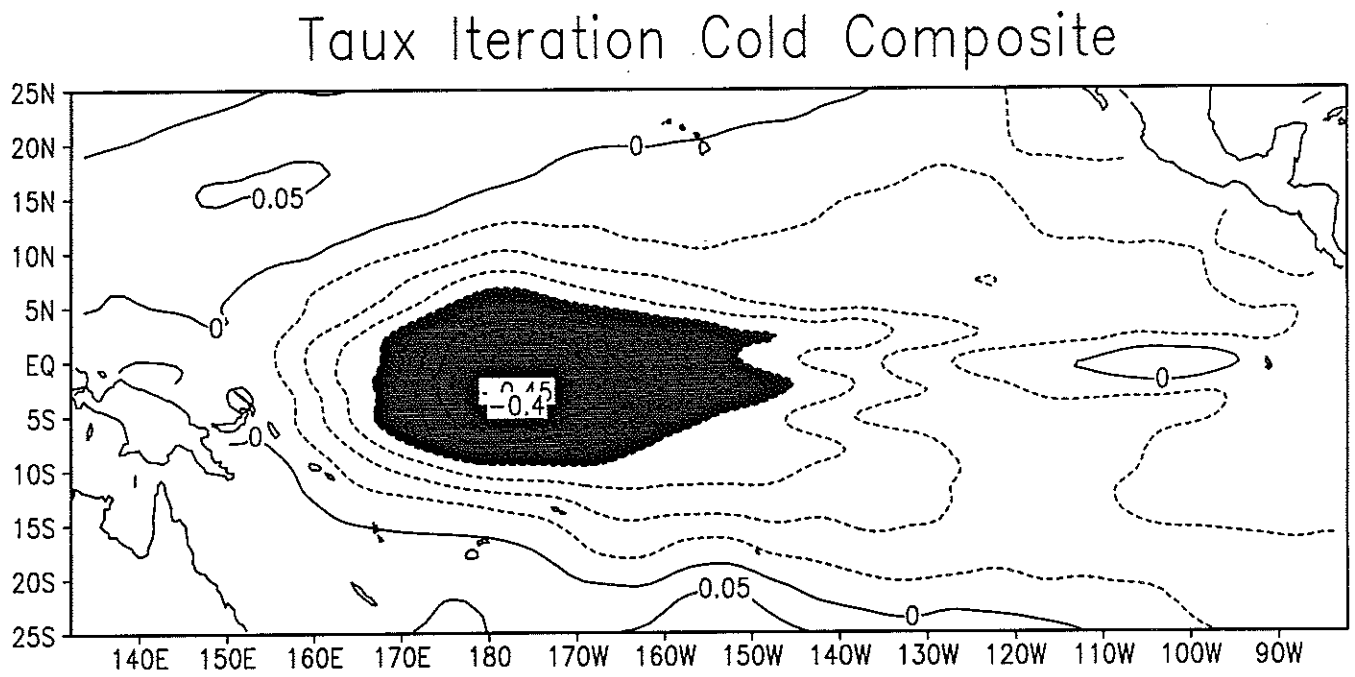
Taux Iteration Cold Composite
25N
20N
15N
10N
5N
EQ
5S
10S
15S
20S
25S
140E
150E
160E
170E
180
170W
160W
150W
140W
130W
120W
110W
100W
90W
0
0.05
-0.4
0.05

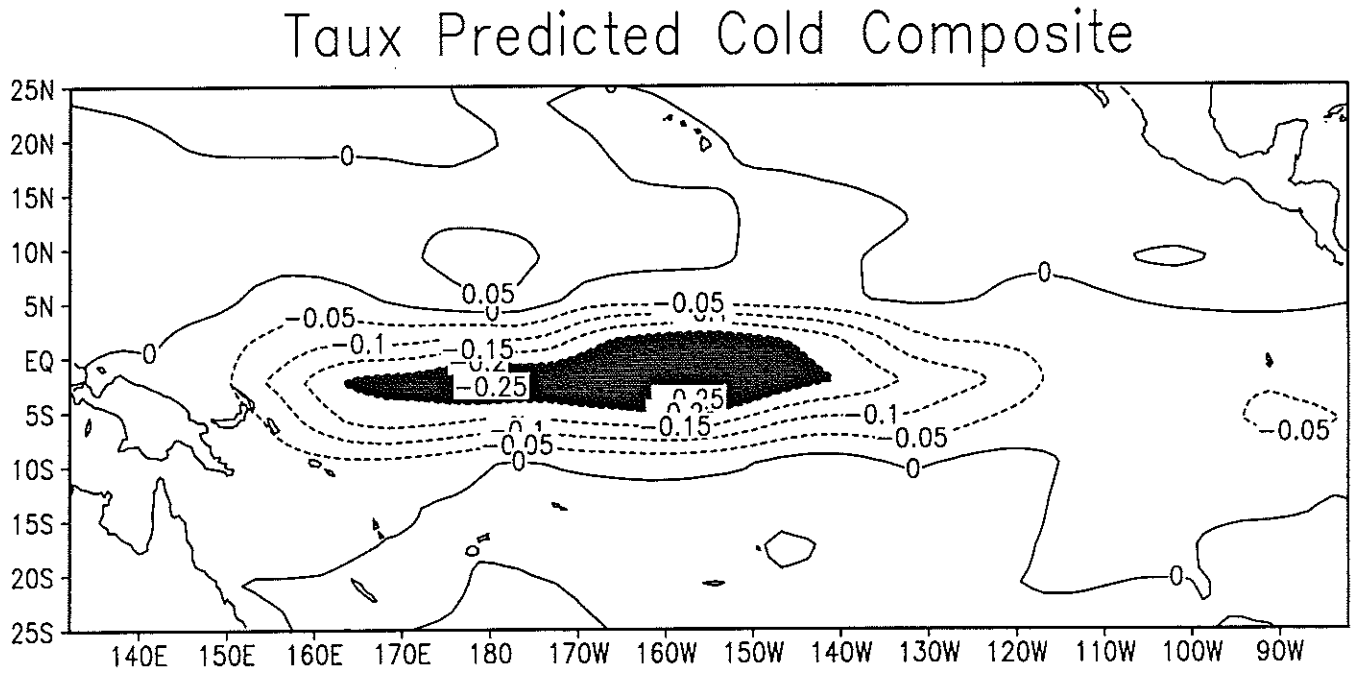
Taux Predicted Cold Composite
25N
20N
15N
10N
5N
EQ
5S
10S
15S
20S
25S
140E
150E
160E
170E
180
170W
160W
150W
140W
130W
120W
110W
100W
90W
0
0.05
-0.05
-0.1
-0.15
-0.25
-0.05

Figure 17

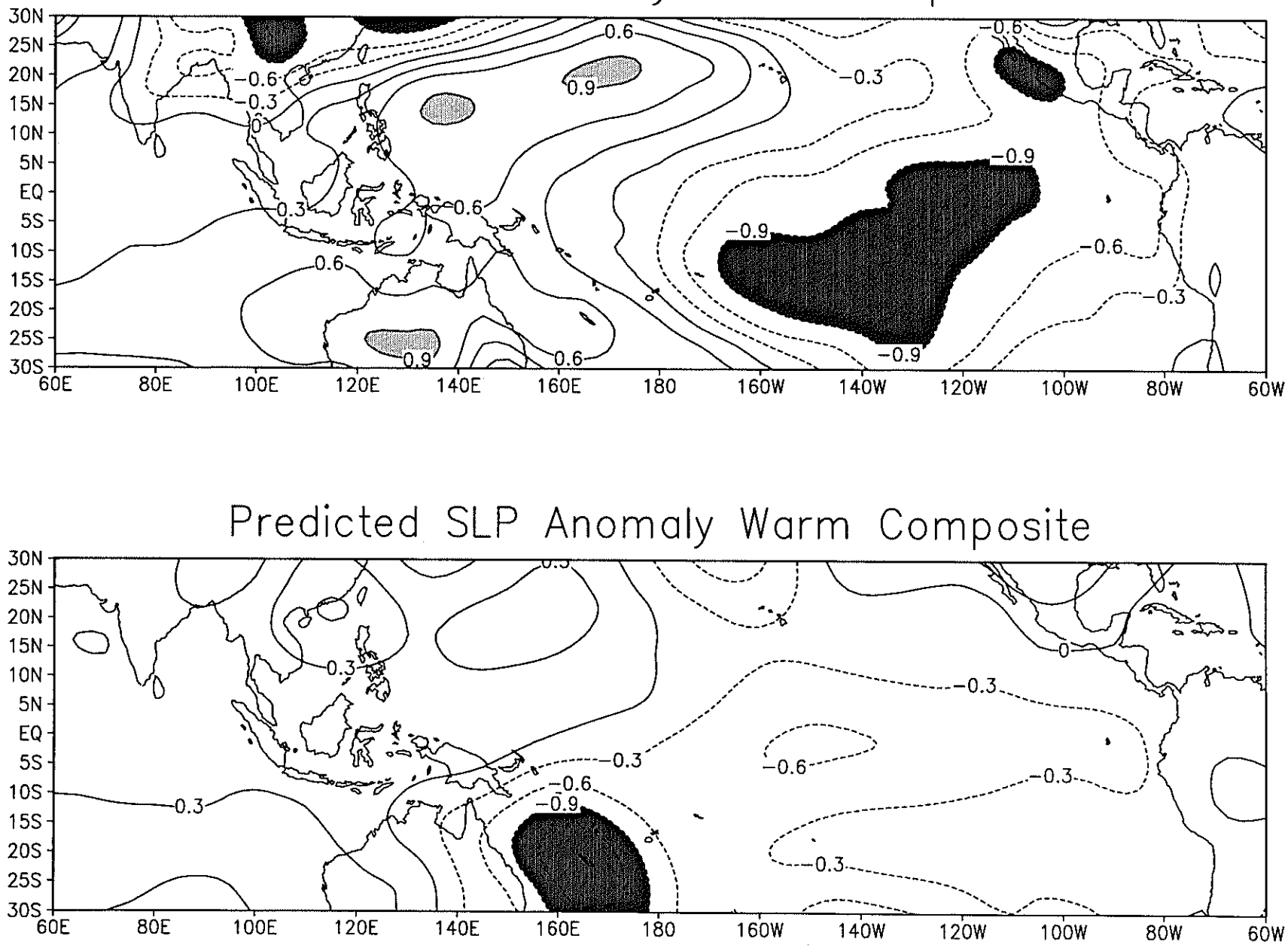
C20C SLP Anomaly Warm Composite
30N
25N
20N
15N
10N
5N
EQ
5S
10S
15S
20S
25S
30S
60E
80E
100E
120E
140E
160E
180
160W
140W
120W
100W
80W
60W
0.6
0.9
-0.6
-0.3
0
0.3
-0.9
Predicted SLP Anomaly Warm Composite
30N
25N
20N
15N
10N
5N
EQ
5S
10S
15S
20S
25S
30S
60E
80E
100E
120E
140E
160E
180
160W
140W
120W
100W
80W
60W
0.3
0
-0.3
-0.6
-0.9

Figure 18

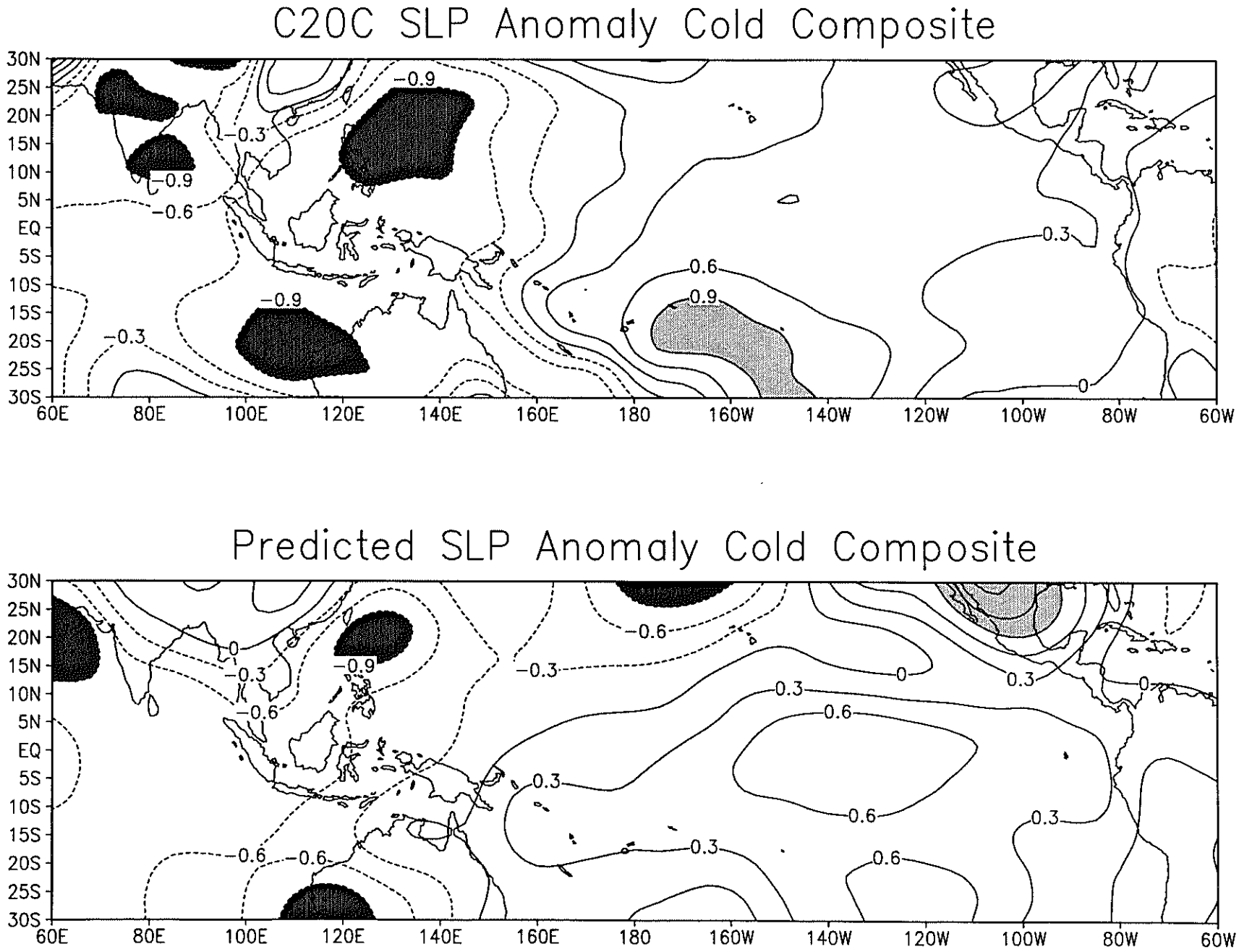
C20C SLP Anomaly Cold Composite
30N
25N
20N
15N
10N
5N
EQ
5S
10S
15S
20S
25S
30S
60E
80E
100E
120E
140E
160E
180
160W
140W
120W
100W
80W
60W
−0.9
−0.3
−0.9
−0.6
−0.9
−0.3
0.3
0.6
0.9
0
Predicted SLP Anomaly Cold Composite
0
−0.3
−0.9
−0.6
−0.6
−0.3
0
0.3
0
0.3
0.6
0.3
0.6
0.3
0.6
−0.6
−0.6
0.3
0.6

Figure 19

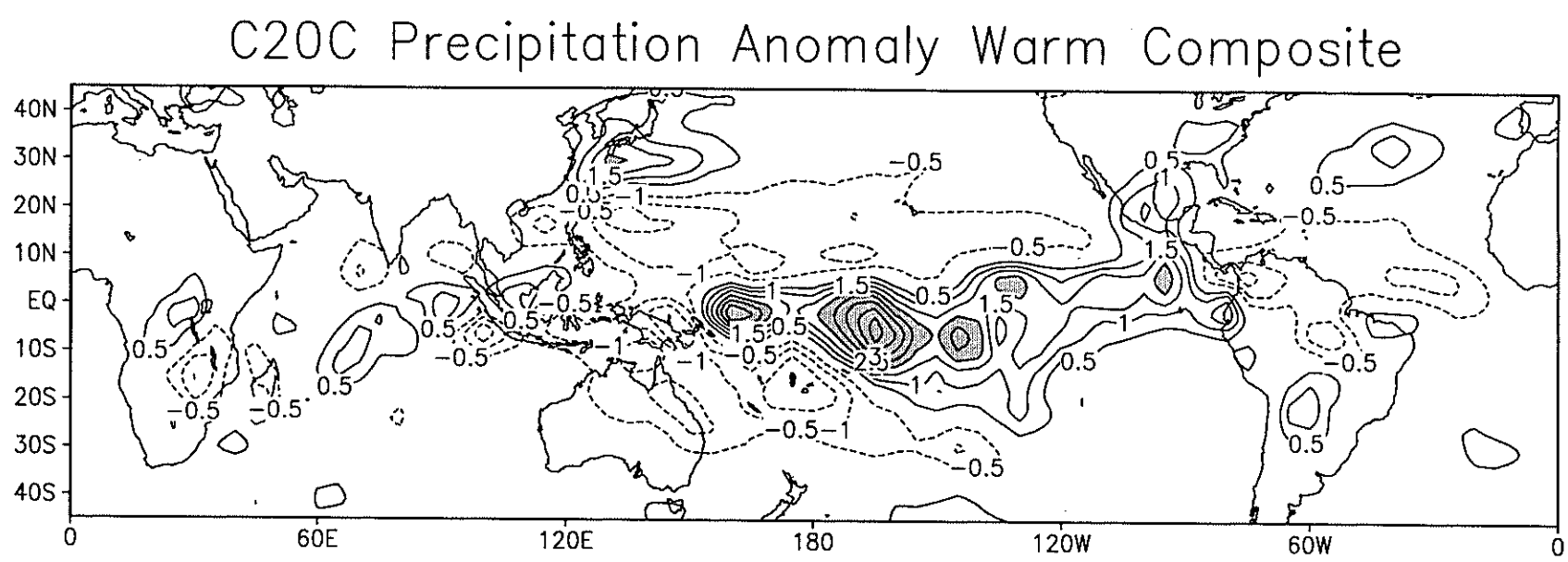
C20C Precipitation Anomaly Warm Composite
40N
30N
20N
10N
EQ
10S
20S
30S
40S
0
60E
120E
180
120W
60W
0

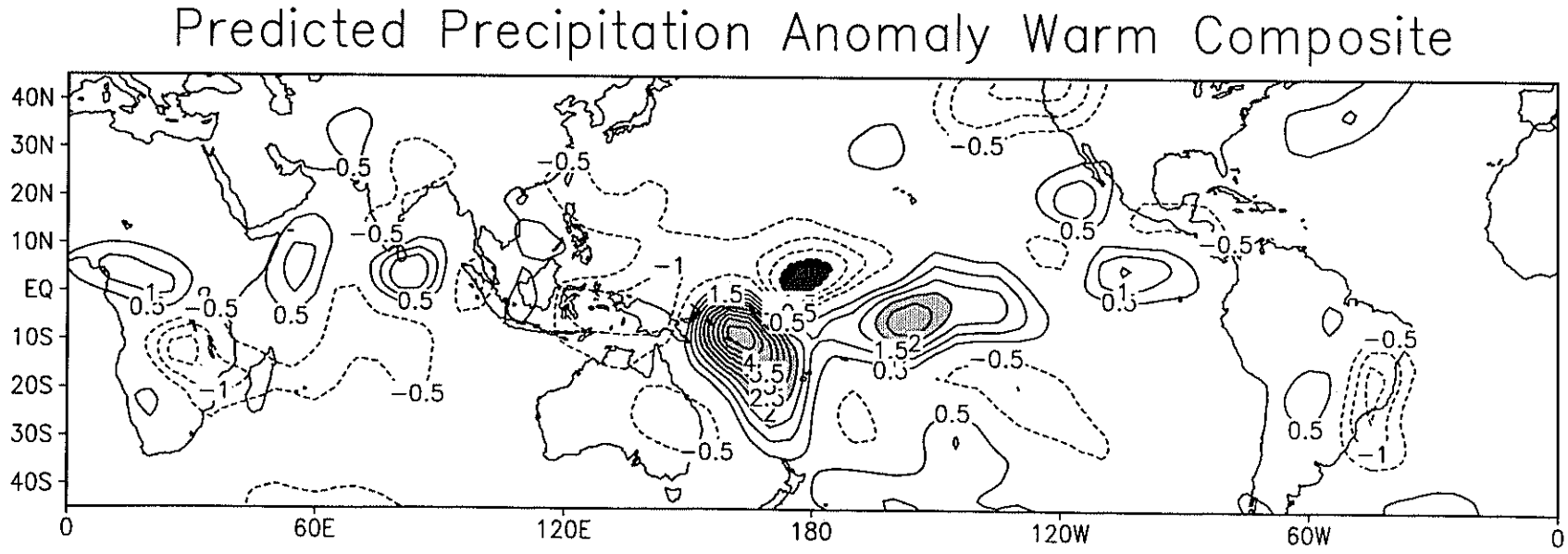
Predicted Precipitation Anomaly Warm Composite
40N
30N
20N
10N
EQ
10S
20S
30S
40S
0
60E
120E
180
120W
60W
0

Figure 20

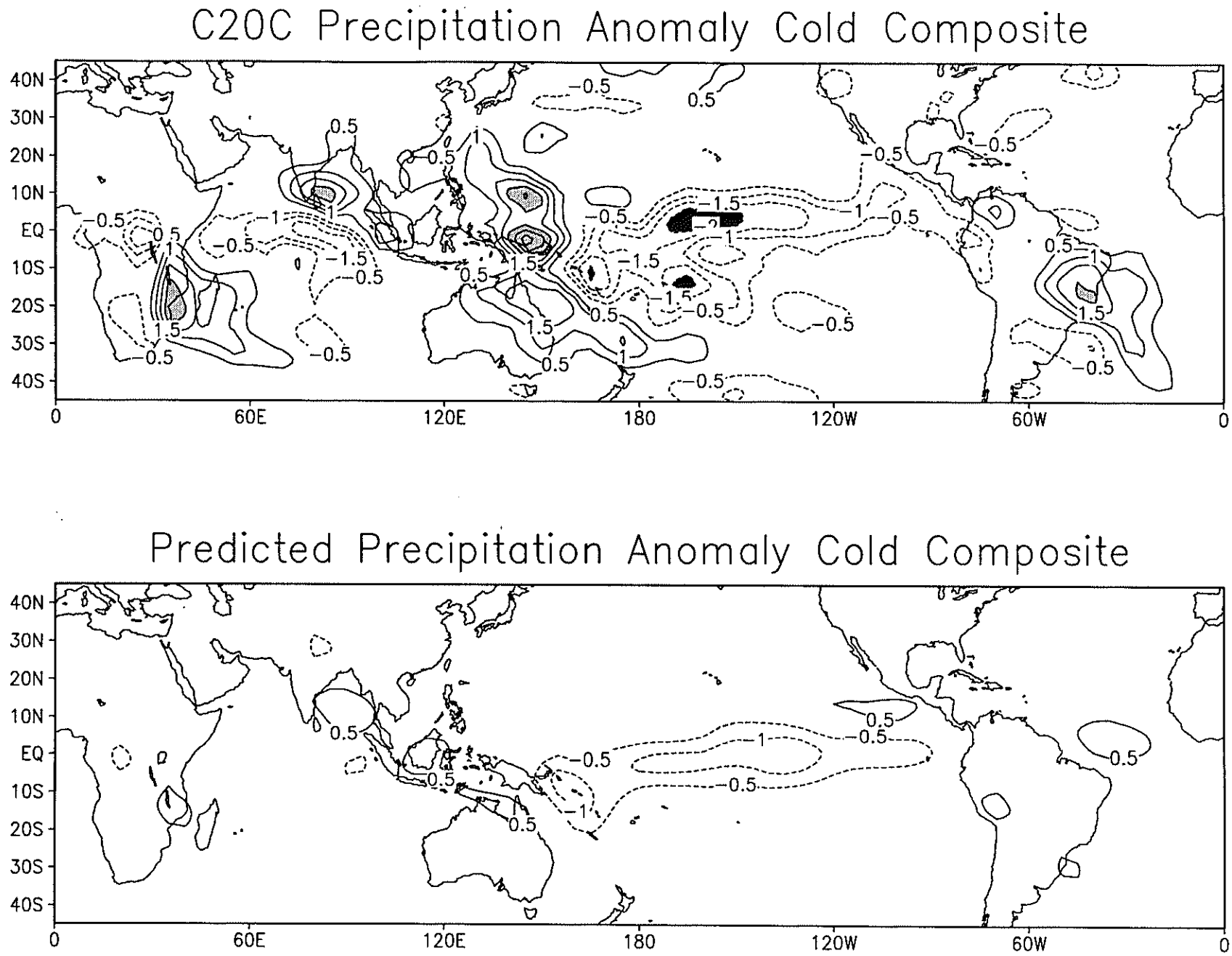
C20C Precipitation Anomaly Cold Composite
40N
30N
20N
10N
EQ
10S
20S
30S
40S
0
60E
120E
180
120W
60W
0
Predicted Precipitation Anomaly Cold Composite
40N
30N
20N
10N
EQ
10S
20S
30S
40S
0
60E
120E
180
120W
60W
0

Figure 21